The *Neuropteris ovata* frond and its cyclopteroids: micromorphology-spectrochemistry-fractal taxonomy: Propositions for restructuring and taxonomy (Pennsylvanian, Canada)

ERWIN L. ZODROW, JOSÉ A. D'ANGELO & CHRISTOPHER J. CLEAL

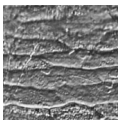

The primary study material consists of the 65-cm frond *Neuropteris ovata* (Hoffmann) var. *simonii*, associate petiole with organically attached cyclopteroid leaflets and trunk. Ancillary *N. ovata* material is used, all from the Asturian–Cantabrian strata of the Sydney Coalfield, Canada. This material is appropriate for the objective of the study to present an *ovata*-frond Aufbau in terms of micromorphology coupled with chemistry using an holistic sampling design (co-ordinating epidermal microscopy with chemistry per sample location). Chemical analyses were obtained by the reliable FTIR technique (Fourier transform infrared spectroscopy) and interpreted via chemometrics by methods of principal component analysis. Fractal geometry is introduced as a promising taxonomic parameter. The main conclusions include that the *N. ovata* plant can be characterized by three distinct epidermal structures: (1) rectangular elongate (trunk and petiole), (2) elongate (rachides of three orders), and (3) undulate (pinnule), which to a certain extent agrees with the chemistry of the frond Aufbau. The frond was also complex – architecturally, histologically, physiologically, chemically and autecologically. It was photosynthetic, had secretory organs (implying a characteristic plant aroma), supporting rodlets, divers epicuticular features, and a distinct chemical composition/structure. The frond was likely 4 m long with complex-pinnate cyclopteroid leaflets, fimbriate or entire-margined, below and above the main bifurcation, which begs the question of cyclopteroid definition and function. The overall results will be beneficial to taxonomy/systematics, and guide pteridospermous reconstruction into a new paradigm. • Key words: morphology-chemistry, cyclopteroids, frond Aufbau, foliage, linkage, reconstruction.

ZODROW, E.L., D'ANGELO, J.A. & CLEAL, C.J. 2016. The *Neuropteris ovata* frond and its cyclopteroids: micromorphology-spectrochemistry-fractal taxonomy: Propositions for restructuring and taxonomy (Pennsylvanian, Canada). *Bulletin of Geosciences 91(4)*, 669–704 (18 figures, 10 tables, supplementary materials). Czech Geological Survey, Prague. ISSN 1214-1119. Manuscript received March 18, 2016; accepted in revised form October 13, 2016; published online January 13, 2017; issued February 7, 2017.

Erwin L. Zodrow, Palaeobiology Laboratory, Cape Breton University, Sydney, Nova Scotia, Canada; zzodrovii@gmail.com • José A. D'Angelo (corresponding author), the same address as the first author, and IANIGLA-CCT-CONICET-Mendoza-Área de Química, FCEN, Universidad Nacional de Cuyo, M55002JMA Mendoza, Argentina; joseadangelo@yahoo.com • Christopher J. Cleal, Department of Biodiversity & Natural Sciences, National Museum Wales, Cathays Park, Cardiff, CF10 3NP, UK; Chris.Cleal@museumwales.ac.uk

Neuropteris ovata (Hoffmann) is one of the most widely recorded medullosalean foliage from the late Carboniferous strata of Euramerica, occurring mostly as compressed pinnate fragments. It has played a major role in the development of the Euramerican Carboniferous plant-fossil biostratigraphy, *i.e.*, the Heerlen biostratigraphy (Laveine 1967; Saltzwedel 1968, 1969; Wagner 1984; Cleal & Thomas 1994), with its earliest appearance being taken as a key indicator for the base of the Westphalian D (Asturian) Substage (*e.g.*, Jongmans 1952, Bode 1958, Darrah 1969, Laveine 1977, Zodrow & Cleal 1985). The species was erected by Hoffmann (*in* Keferstein 1826), based on Westphalian D fragmentary compressions from Piesberg, Osnabrück, Germany (Saltzwedel 1969, Klassen 1984), in which the degree of coalification was too high for cuticular preservation (Cleal & Zodrow 1989). Initial micromorphological (cuticular) studies based on detached, compressed (coalified) pinnules from other areas (*e.g.*, Saar-Lorraine, France/Germany) were done by Gothan (1913, 1916), Barthel (1962), Florin (1925) who described a detached round-margined cyclopteroid pinnule with typical *N. ovata* micromorphology, and by Cleal & Zodrow (1989), and by D'Angelo & Zodrow (2015, 2016) from the Sydney Coalfield, Canada (Fig. 1), among others. In the Sydney Coalfield

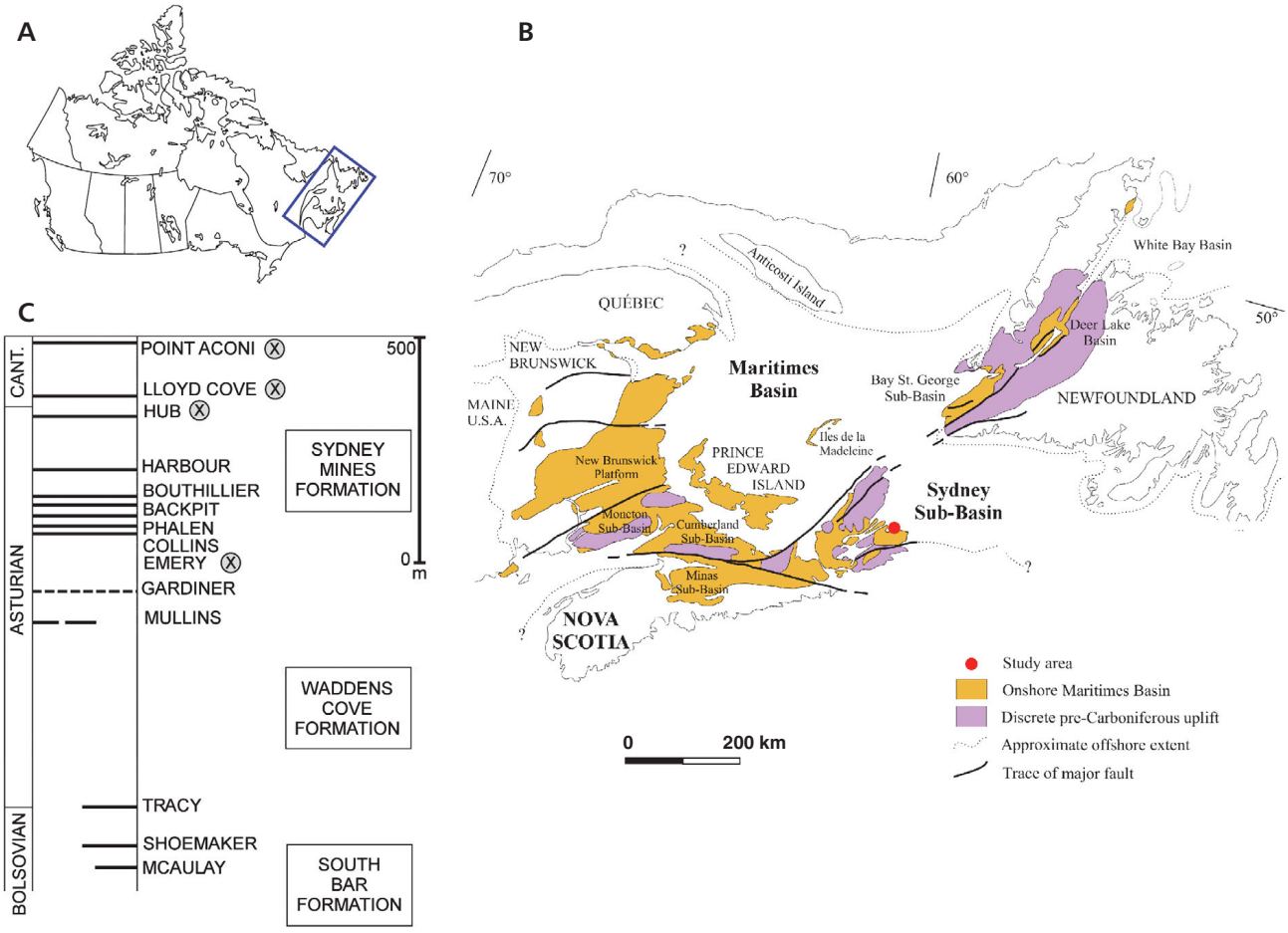

Figure 1. Location map. • A – Maritime Canada (boxed). • B – Maritimes (Carboniferous) Basin. • C – coal lithostratigraphy, Sydney Coalfield. CANT = Cantabrian strata. Sampled roof rocks of coal seams are marked ("X").

well-preserved uni- and bipinnate structures, rarely abscissed pinnules, of *N. ovata* were described by Bell (1938, Fig. 2) from the geological section between the McLean and the Pt. Aconi Seams. Material collected from some of Bell's sample locations provided data for a number of studies concerning different aspects of the species (see Supplementary materials). However, the 65-cm specimen from the Point Aconi Seam (Fig. 1C), interpreted as a bifurcating, overtopped frond, is the largest *N. ovata* sample from the Sydney Coalfield (Zodrow & Cleal 1988, pls 2 and 3, text-fig. 10). In 1989, Cleal & Zodrow proposed a new varietal name for it, *viz. Neuropteris ovata* Hoffmann *in* Keferstein (1826) var. *simonii* (Bertand 1930), partly because of the uncertainty as to whether the plant that produced the Piesberg *N. ovata* type material would have had the same micromorphological (especially epidermal) features as those that produced the cuticles in the 65-cm Sydney specimen. An up-to-date list of varietal *N. ovata* taxa is proposed by Šimůnek & Cleal (2016).

The overall objective of this paper is to further explore the relationship between morphology and chemistry (*cf.* D'Angelo & Zodrow 2016), with focus on the putative cyclopteroid-leaflets problem (1) their positions in the frond, and (2) leaflet morphology, which is underpinned by the micromorphological study. That the form and the chemical composition of plants are related have been presumed in neobotany for over 200 years, originating probably with Linnaeus (see de Candolle 1804, respectively 1816), and have been studied since (*cf.* Hegnauer 1986, and others). However, Rochleder (1854, p. 308) formulated the maxim that for botanical studies "…The botanist cannot do without chemistry, and the chemist without botany" (see commentaries by Greshoff-Haag 1893). To note is that the pharmaceutical science is the real trail-blazer for chemotaxonomy of the extant plant kingdom. In respect to our fossil work, we hypothesize that a similar relationship existed between the medullosalean frond Aufbau and its chemistry (D'Angelo & Zodrow, unpublished data), implying that not the frond morphology on its own, but the chemistry of the morphology is the key for reconstruction and advancing evolutionary systematics. Accordingly, the holistic sampling design used co-ordinated from known locations

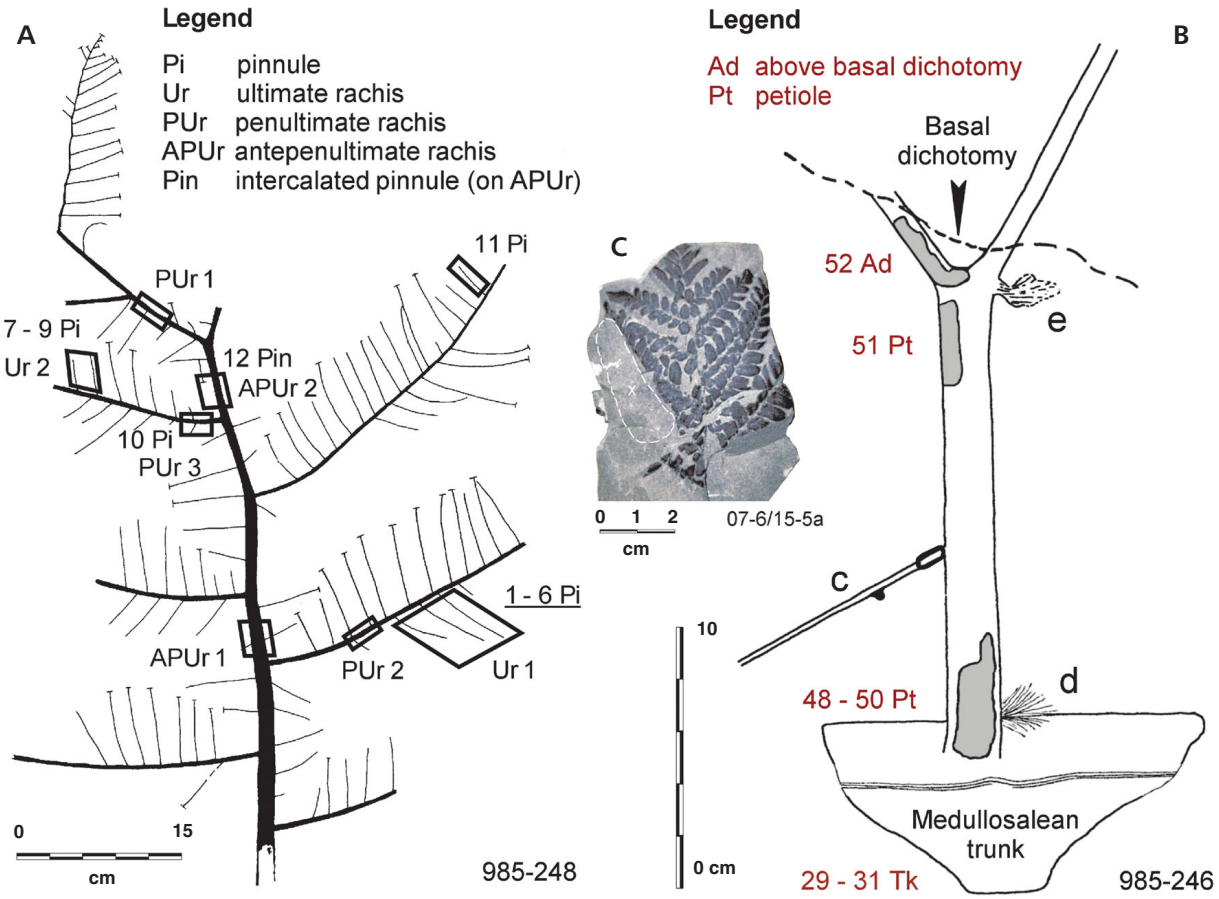

Figure 2. *Simonii* frond and acronyms consistently used for its architectural parts, and a *Neuropteris ovata* var. *simonii* specimen. • A – rachial architecture of the *simonii* frond. Small cross bars signify ultimate (intercalary) pinnae complete with the terminal pinnule. • B – basal dichotomy organically connected? with a trunk fragment. For cyclopteroid leaflet "e" see Fig. 9D to F, and for 52Ad to 29–31Tk see Fig. 9A–C. "ID" numbers preceding Pi, Pin, Ad, Pt and Tk, are explained in the text. • C – a *Neuropteris ovata* var. *simonii* specimen 07-6/15-5a likely representing the tip of a PUr. Cuticles originated from the area marked "X".

(1) the micromorphological data from the 65-cm specimen, the associated petiole, trunk, cyclopteroid leaflets, and from ancillary *N. ovata* material, with (2) the semi-quantitative chemistry by FTIR (D'Angelo & Zodrow, unpublished data). Whereas (2) provided the data for chemometrics, both (1) and (2) and fractal geometry constituted the interpretable data base including, but not restricting to, the relevance of sub- and supradichotomous positions of the cyclopteroid leaflets and size consideration of the *N. ovata* frond *sensu lato*. This in turn has implications for frond reconstruction in more natural terms for the hypothesis of transitory evolution of *Neuropteris* to *Odontopteris* (summaries: Zodrow & Cleal 1988, Laveine 1997).

Acronyms, sample material, preservation, and Ro% (random)

Following, the 65-cm frond together with associated petiole and trunk (Fig. 2A, B) will be referred to as the *simonii* frond to distinguish it from the detached, ancillary pinnate and bipinnate specimens of *N. ovata* var. *simonii*, which are referred to as *simonii* specimens (*e.g.*, Fig. 2C). Acronyms for the architectural frond parts (Pi to Pin, and Ad to Tk) applicable to the entire *simonii* materials are given in Fig. 2A, B. We emphasize that where IR data (from infrared spectra) were obtained from compressions whose extracted cuticles were also figured, the architectural acronyms Pi, Pin, Ad, Pt, Tk, and the two acronyms Co for *Cyclopteris* sp. A Brongniart (982-405) and Cf for *C. fimbriata* Lesquereux (977-443) are preceded by "ID" numbers (*e.g.*, 11Pi) that correspond to variable-input identification in the PCA model (principal component analysis): Table 1, Fig. 16, or Table S1, Supplementary materials. Table 1 also compiled information on the total number of IR spectra in the analysis, cuticular slides prepared, maceration times, and pertinent geological information.

The *simonii* specimens (*e.g.*, Fig. 2C) were included for (1) testing the hypothesis of connectivity of Pi's with [detached] 42–44Co and 45–47Cf by FTIR methodology that

Table 1. IR spectra of compressions, slides of cuticles, maceration, lithology, and Ro%. [a] See Fig. 16 or Table 1S (Supplementary materials); [b] D'Angelo & Zodrow (2016); [c] Cleal & Zodrow (1989); [d] Zodrow & Cleal (1988); [e] n.a. not available.

Specimen Species PCA input ID[a]	In the present study compression spectra	Slides	Maceration hour (h) minute (min)	Facies	Coal Seam meter (m) above	Ro% (No. samples)
Simonii frond: Fig. 2A				Micaceous fine-grained		
1–11Pi	11[b]	22	5 min to 2 h 40 min	Sandstone	Pt. Aconi	0.79 ± 0.028
12Pin	1[b]	–	3 h to 6 h	"	(3.5)	(1)
Ur	None	7	3 h to 6 h	"	"	"
Pur	None	12	3 h to 6 h	"	"	"
APUr	None	8	3 h to 6 h	"	"	"
Medullosalean trunk: Fig. 2B						
29–31Tk	3	4	5 h	"	Pt. Aconi	0.80 ± 0.54
					(3.5)	(19)
Simonii specimens						
979-230		pl. 99, 3–4[c]		Mudstone	Hub	0.72 ± 0.06
32Pi	1	None	Not recorded		(unknown)	(9)
982-405		pl. 98, 2; 99, 2[c]		Thinly	Pt. Aconi	n.a.[e]
33–35Pi	3	None	Not recorded	Laminated Shale	(1)	
982-405	2–3 mm below specimen	pl. 98, 2[c]		Thinly	Pt. Aconi	n.a.
36–38Pi	3	3	5 h to 6 h	Laminated	(1)	
Ur	None	1	6 h	Shale		
07-6/15-5a: Fig. 2C				Massive	Hub	n.a.
39–41Pi	3	7	3 h 15 min to 26 h	Shale	(unknown)	
Ur	None	1	5 h 30 min			
Cyclopteris sp. A Brongniart,	Detached					
982-405	2–3 mm below specimen	pl. 98, 2[c]		Thinly	Pt. Aconi	n.a.
42-44Co	3	8	6 h to 41 h 15 min	Laminated	(1)	
Ur	None	3	6 h	Shale		
Cyclopteris fimbriata Lesquereux,	Detached		pl. 4, 3[d]	Silty shale	Emery	0.84 ± 0.021
977-443					(0.4)	(19)
45-47Cf	3	9	4h			
Basal bifurcation and petiole, attached to a trunk: Fig. 2B						
985-246			pl. 4, 1a[d]	Micaceous	Pt. Aconi	n.a.
48-50Pt	3	8	3h	Fine-grained	(3.5)	
51Pt	1	None		Sandstone		
52Ad	1	2	3h			
"e", attached	None	2		"	"	
"d", attached	None	2				
Totals	36	96				

already had demonstrated its value in such questions (*e.g*. Cleal *et al*. 2010, Zodrow *et al.* 2013), and (2) confirming ultimate-rachial morphology. Table 2 lists the *simonii* specimens that were analyzed.

The *simonii* frond was entombed in sandstone (*cf*. Forgeron *et al.* 1986, and references therein) 3.5 m above the Point Aconi Seam (Zodrow & Cleal 1988, text-figs 3, 4, and pl. 1). Based on field mapping and thin-section analysis, the sandstone matrix is a cross-laminated, very fine to fine-grained, poorly sorted epiclastic arenite (quartzose) sandstone. Although it contains organic debris (kerogen) of undetermined plant origins, pyrite was not observed (Table 3). Cuticles are informative which was mainly due to a favorable thermal history. This is interpreted through lower vitrinite-reflectance values, Ro%, Table 1 (Hacquebard 1984, Gibling *et al.* 2002), *i.e*. Bituminous, High Volatile "A" rank coal (Traverse 2008, fig. 19.2). The applicable Ro% value is equivalent to

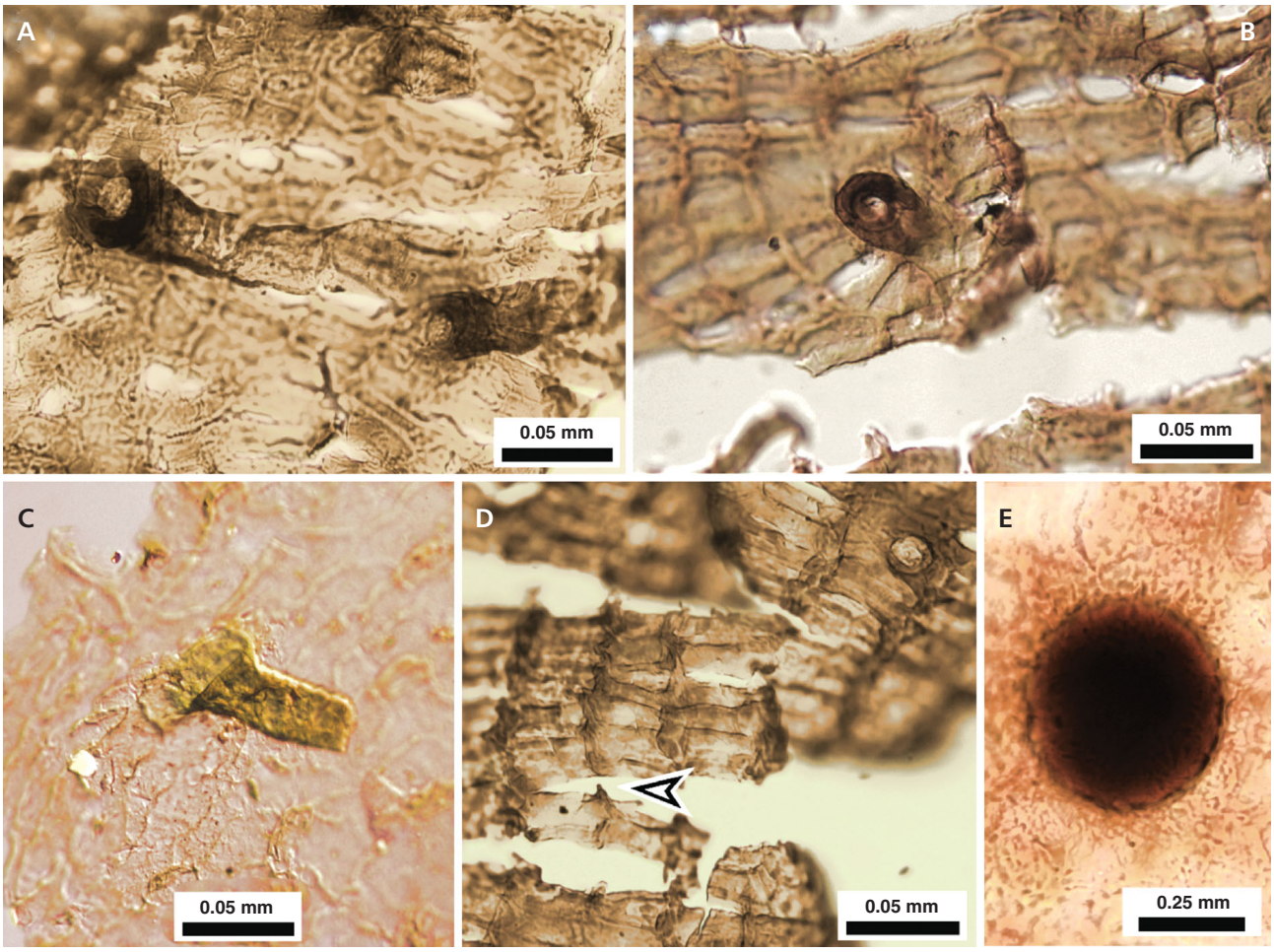

Figure 3. *Neuropteris ovata* var. *simonii*. Illustrating files, trichomes, dentate extensions, and secretory bodies. • A – files, incomplete, collar-ringed base, parallel-margined (*cf*. Fig. 8A, arrowed). • B – file, basal cross section. • C – trichomatous base, *ca* 50 µm, oval-shaped. • D – dentate extensions on anticlinal walls (arrowed). • E – secretory organ. Nomarski phase-contrast condition. Slide documentation: APUr 2 85-248/17 Side 2; PUr 3 85-248/12; Pi 85-248/2; APUr 1 85-248/12; PUr 3 85-248/13 (not shown, slightly below APUr 1), respectively.

a minimum of 28% volatiles (Barthel 1962, 1966). This condition implies IR-data comparability (*cf*. Zodrow *et al.* 2009; Zodrow *et al.* 2013, fig. 4).

All fossil material, generated analytical FTIR data, *ca* 200 micromorphological slides, and nearly 150 digitized image are housed in the Palaeobotanical Collection, Cape Breton University, and curated by E.L. Zodrow.

Cuticular features

Following Fahn's (1979) summary discussion of known angiospermous secretory tissues, we assumed similar features to have existed in the ancient plant fossils, respectively medullosaleans (unpublished research notes, E.L. Zodrow 2015, D'Angelo & Zodrow 2016). Accordingly, as secretory tissues we included: files, trichomes, secretory organs, and hydathodes, defined by the following preservation features.

Files. – Linear, non-segmented, hollow structures, *ca* 20 µm in diameter or less, with a parallel-margined base characterized by an enlarged solid collar, 10–14 µm in diameter (Fig. 3A). Only truncated files were found, minimally 200 µm long and 35 µm wide, which when dislodged or toppled-over, left in their places open and round structural holes 18–60 µm in diameter (modal diameter 34 µm, 39 out of n = 126), at times semi-encircled by cells (Fig. 3B). Compare with Florin's round structural holes in *Cyclopteris* sp. which he called hair bases (1925, pl. 10, figs 11, 12).

Trichomes. – Uniseriate, multicellular, hollow structures with distinctly flared bases, found most frequently truncated, fragmentary, up to 1,000 µm long (Fig. 3C). The base from toppled-over or dislodged trichomes is described as large open, elongate-ovate-obovate (peltate) structure with "ringed collars" (*e.g*., Gothan 1916, Barthel 1962, Cleal & Zodrow 1989). Variable base-lengths, 37–105 µm, probably correlate with developmental stages, where the largest

Table 2. Ancillary specimens for micromorphology/fractal dimension.

Shale slab	Size of shale slab	Glass slide	Taxon	Coal Seam	Detached specimen (size cm)
980-374	11 × 10 cm	80-374/1–3	*C. fimbriata*	8 m above Lloyd Cove	Pinnate, 4 × 3
992-237	60 × 25 cm	92-237/2	*C. fimbriata*	Lloyd Cove	Pinnule, 4
992-237	60 × 25 cm	92-237/3	*Neuropteris triangularis*	Lloyd Cove	Pinnule, 5
992-243	16 × 14 cm	92-243/2	*N. ovata*	Lloyd Cove	Ultimate pinna, 16

Table 3. Mineralogy and X-ray analysis of the sandstone in which the *simonii* frond was entombed. [a]Includes phyllosilicates

Mineral	Relative mineral content	Detrital size range (μm)	Shape
Quartz	Overwhelmingly major	8–200	Very angular
Mica[a]	Major	200–400 × 10–20	Elongate
Feldspar group	Very rare	50–80	Angular
Organics	Fairly abundant	500 × 70	Elongate
Pyrite	Not seen	–	–

Diffractogram of the rock matrix of the *simonii* frond (985-248).

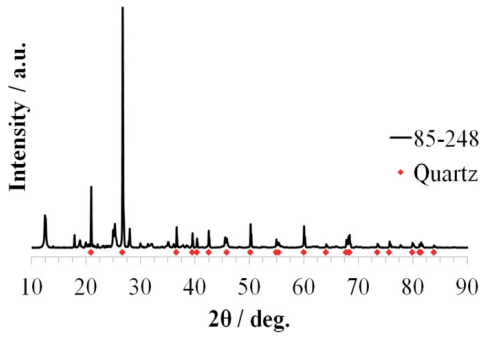

bases likely stemmed from thorn-like structures, rather than trichomes. Truncation and irregular uprooting of structures from pinnules and all-order rachides are most likely related to cover-slide preparation, including HF liberation from the rock matrix (see Supplementary materials). A taphonomic origin cannot be ruled out.

Secretory organs. – Round and opaque, *ca* 10–100 μm in diameter (*e.g.*, Fig. 3E). They occurred prolifically over the entire *simonii* material without preferred orientation (Zodrow *et al.*, 2016).

Hydathodes (cf. Cleal & Shute 2012). – The round-like, structural holes aligned particularly along the margins of abaxial cuticles (*e.g.*, Fig. 11A) may represent hydathodes (rather than trichomes/files?). Definitive structural-identification criteria have as yet not been established, except for the alignment at pinnule margins as is found in angiosperms.

"Dentate" extensions occurred generally on the shorter, antliclinal walls of PUr and APUr surfaces with elongate cells (*e.g.* Fig. 3D: see cuticles of *Cordaites* spp., Zodrow *et al.* 2000, fig. 3d). On Ur surfaces, "dentate" extensions are minor and generally non-obstructive to viewing micromorphological features. These cutinized extensions were squeezed between anticlinal-cell walls, and when observed in extant flora are interpreted as prominent xeromorphic features. The "teeth" point inwards (compare with Braune *et al.* 1999, Abb. 67). This feature may be difficult to spot on cover-slide preparations, but crinkly and relatively thick cutinized anticlinal walls usually signal their presence.

A stoma consisting of only two guard cells is referred to as anomocytic (Fig. 15A), and as brachyparacytic if a pair of lateral subsidiary cells is present (stippled in Fig. 15B).

Methods

Preparing the compression material for IR analysis

Pi compressions from the *simonii* specimens, and the *simonii* frond were HF (48%)-liberated, whereas APUr, PUr, Tk, Ad and Pt compressions were hand-lifted from the rock matrices incurring some fracturing. However, certain cyclopteroid leafletss (i) *C. fimbriata*, 2-366, Lloyd Cove Seam, disintegrated on HF treatment, and (ii) *C. fimbriata,* 82-405C.fim2 (co-occurring with *Cyclopteris* sp. A: Table 1), only yielded rachial cuticles (Fig. 14A–D). The two specimens are not listed in Tables 1 and 2. Removal of pinnule midveins for FTIR analysis (Zodrow & Mastalerz 2001, fig. 7C, D), was not necessary, as the Ur cells divided into 2–3 strands prior to entering the Pi base (Fig. 4A). A Ur compression with trichomes/files is shown in Fig. 4B.

Liberated PUr and APUr compressions were further HF-treated for up to 2.5 hours to remove infilled-rock matrix. Tracheids were not preserved. The Tk specimens, because of complex preservation, required further HF treatment to obtain compressions free of rock debris. All compressions were washed in distilled water for at least two days to eliminate acidic and other chemical residuals. Hand-picked compressions were then subdivided into *ca* 80 : 20 proportions of which the larger one was air-dried exclusively for IR analysis, and the smaller one wet-transferred for maceration and micromorphological analysis (see Supplementary materials). Recovered cuticles were

teased apart, when possible, cover-glass mounted and studied under a binocular microscope equipped with Nomarski phase-contrast filters and digital-imaging capabilities.

Morphometric measurements were routinely made at ×250 magnification. We consistently obtained relatively more accurate measurements from more surfaces with near-isodiametric cells than from surfaces opposite with medial cell splitting and cutinized dentate walls. The reason for this is that the former is less cutinized and the dentate features do not obscure anticlinal walls. To note is that only non-split cells were measured (Ur, PUr, and APUr), see later.

Compression FTIR and spectral interpretation

Methodology. – Although generally ignored in palaeobotany as a valuable research method (*cf.* Heredia-Guerrero *et al.* 2014, Chen *et al*. 2015), IR spectra underpinned the conclusions of this study. The spectra were obtained from 250 mg KBr pellets with thoroughly ground 0.8–1.4 mg of compression samples. Co-added were 256 interferograms with a standard resolution of 4 cm^{-1} wavenumber in the range 4000 cm^{-1} to 400 cm^{-1}. For basic information and FTIR nomenclature see Smith (1996) or Chen *et al*. (2015) and references therein.

IR information is found in three spectral zones with which we are familiar from our long-study history of medullosalean compression/cuticle spectra, dating back to Lyons *et al.* (1995). In principle, many different functional groups could be absorbing in these three zones. We named them: (1) hydroxyl and aliphatics zone (3700–2600 cm^{-1}), using the 3000–2650 cm^{-1} region instead of the 720–700 cm^{-1} band for calculation (see later), (2) oxygen containing and aromatic zone, some aliphatics, too (1800–1000 cm^{-1}), and (3) aromatic zone (900–700 cm^{-1}).

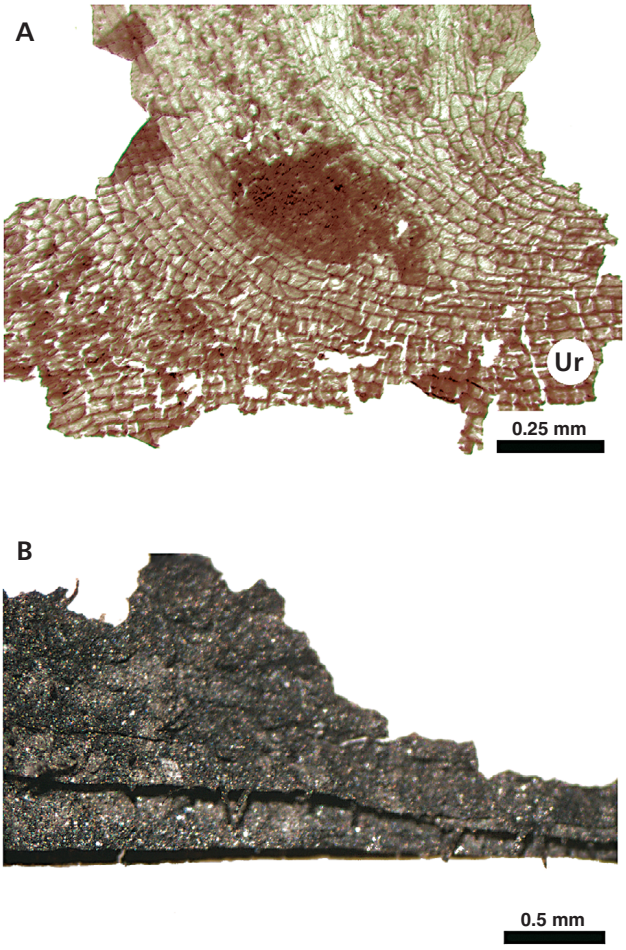

Figure 4. *Neuropteris ovata* var. *simonii.* • A – a decurrent midvein on an Ur. • B – Ur compression positioned obliquely on edge to view coalified trichomes/files on the abaxial surface. Photographed in water. Slide documentation: 07-6/15-5a-5b; T(emporary) slide 07-6/15-5a, respectively.

Table 4. Wavenumber ranges in which the main functional groups and classes of compounds absorb infrared radiation. Abbreviation: [a] According to Colthup *et al.* (1990), Petersen & Nytoft (2006), Petersen *et al.* (2008), D'Angelo & Zodrow (2011), and D'Angelo *et al.* (2011). [b] It should be noted that the peak at 2925 cm^{-1} (obtained after deconvolution of aliphatic C-H stretching region, not shown) represents the contribution from CH_3 and CH_2 groups attached directly to aromatic rings (see Petersen & Nytoft 2006).

Range (cm^{-1})[a]	Group and class of compound	Assignment
3450–3250	Hydroxyl (-OH) in alcohols and phenols	O-H stretch
3100–3000	=CH in aromatic and unsaturated hydrocarbons	=C-H stretch
2936–2913	Methylene and methyl (CH_3-, CH_2-) in aliphatic compounds [b]	CH_3-, CH_2- antisymmetric stretch
2864–2843	CH_3-, CH_2- in aliphatic compounds	CH_3-, CH_2- symmetric stretch
1724–1695	Carbonyl (C=O) in carboxylic acids, ketones	C=O stretch
1660–1650	C=O in highly conjugated ketonic structures	C=O stretch
1620–1498	Benzene ring in aromatic compounds	C=C aromatic ring stretch
1449–1435	CH_3-, CH_2- in aliphatic compounds	CH_3 antisymmetrical or CH_2 scissor deformation
1279–1250	C-O in aromatic ethers	C-O stretch
1040–1027	C-O-C in aliphatic ethers, Si-O in silicates	C-O-C antisymmetric stretch, Si-O stretch
900–700	=CH in aromatic hydrocarbons	=C-H out-of-plane bending

Table 5. Definition of semi-quantitative area ratios derived from FTIR spectra.

#	Ratio PCA variable	Band-region (cm^{-1}) Band-region ratios	Interpretation and remarks
1	CH_2/CH_3	3000–2800	Methylene/methyl ratio. It relates to aliphatic chain length and degree of branching of aliphatic side groups (side chains attached to macromolecular structure; Lin & Ritz (1993a, b). A higher value implies comparatively longer and straight chains, a lower value shorter and more branched chains. Caution is advised using the ratio, as it may be misleading due to the contribution from CH_2 and CH_3 groups attached directly to aromatic rings (Petersen & Nytoft 2006).
2	CH_{al}/Ox	(3000–2800) / (1800–1600)	Aliphatic/oxygen-containing compounds ratio. Relative contribution of aliphatic C-H stretching bands (CH_{al}) to the combined contribution of oxygen-containing groups and aromatic carbon (Ox). From higher values decreasing oxygen-containing groups can be inferred, or the lower the CH_{al}/Ox ratio, the higher the Ox term. This ratio could provide some information about oxidation in organic matter (*e.g.*, Mastalerz & Bustin 1997, Zodrow & Mastalerz 2001).
3	C=O/C=C	(1700–1600) / (1600–1500)	Carbonyl /aromatic ratio of carbon groups. Relative contribution of C=O to aromatic carbon groups. Higher values indicate increasing carbonyl/carboxyl groups to aromatic carbon groups (D'Angelo 2006).
4	C=O cont	(~1714) / (1800–1600)	Carbonyl contribution. Relative contribution of carbonyl/carboxyl groups (C=O; peak centered near 1714 cm^{-1}) to combined contribution of oxygen-containing groups and aromatic carbon (C=C) structures.
5	C=C cont	(~1600) / (1800–1600)	Aromatic carbon contribution. Relative contribution of aromatic carbon groups (C=C; peak in 1650 to 1520 cm^{-1} region, centered near 1600 cm^{-1}) to combined contribution of oxygen-containing groups and aromatic carbon (C=C) structures.
6	CH_{al}/C=C	(3000–2800) / (1600–1500)	Aliphatic/aromatic carbon groups ratio. Relative contribution of aliphatic C-H stretching bands to aromatic carbon groups (C=C). Higher values indicate increasing aliphatic groups to aromatic carbon groups. This ratio is equivalent to the I1 index of Guo & Bustin (1998).
7	"A" factor = $CH_{al}/(CH_{al}+C=C)$	(3000–2800) / [(3000–2800) + (1600–1500)]	Relative contribution of aliphatic C-H stretching bands to sum of aliphatic C-H stretching and aromatic carbon structures. According to Ganz & Kalkreuth (1987) it represents change in relative intensity of aliphatic groups.
8	"C" factor = Ox / (Ox+C=C)	(1800–1600) / [(1800–1600) + (1600–1500)]	Relative contribution of oxygen-containing compounds to the sum of oxygen-containing structures and bands of aromatic carbon. According to Ganz & Kalkreuth (1987) it represents change in carbonyl/carboxyl groups.
9	CH_{al}/C=O	(3000–2800) / (1800–1700)	Aliphatic / carbonyl groups ratio. Relative contribution of aliphatic C-H stretching bands to carbonyl/carboxyl groups (C=O). Indicator for cross-linking degree of a polymeric structure (*i.e.*, the linking of polymer chains). Lower values indicate higher C=O content and higher cross-linking (Benítez *et al*. 2004).
10	CH_{ar}/CH_{al}	(900–700) / (3000– 2800)	Aromatic C-H out-of-plane bending/aliphatic ratio. Contribution of aromatic C-H out-of-plane bending modes to aliphatic C-H stretching bands (aliphatic H bands). Indicator for aromaticity in organic matter. Higher values indicate higher aromaticity, *i.e.*, higher content of aromatic groups *vs* aliphatic groups.
11	CH_{ar}/C=C	(900–700) / (1600– 1500)	Aromatic C-H out-of-plane bending/aromatic carbon groups ratio. Ratio of integrated area of aromatic C-H out-of-plane bending deformations to those of aromatic carbon groups. Used as measure of the degree of condensation of aromatic rings.

Repetitive assignation of aromatics and other functional groups in the latter two zones is the result of different possible energies of absorption (spectral wavenumbers) for a single functional group.

For maximal IR information, spectra were analyzed in two complementary ways: (i) qualitatively, and (ii) semi-quantitatively. (i) Included assignments of salient IR bands to groups and classes of compounds (Table 4) which were applicable to all of the spectra in the study. (ii) Involved mathematical techniques for calculating semi-quantitative chemical ratios from the digitized spectra. This not only maximized information for interpreting mixed organic samples (compression, cuticle), but also assured direct comparability with our previously published data. (ii) Also constituted the input-data matrix for the chemometric analysis. In effect, we subscribed (*cf*. Westad 2000) to the new taxonomy espoused by Wheeler (2008).

Our IR interpretive interest focused on PC (principal-component) scores, obtained after complexity reduction, which is one objective of the multivariate analysis for

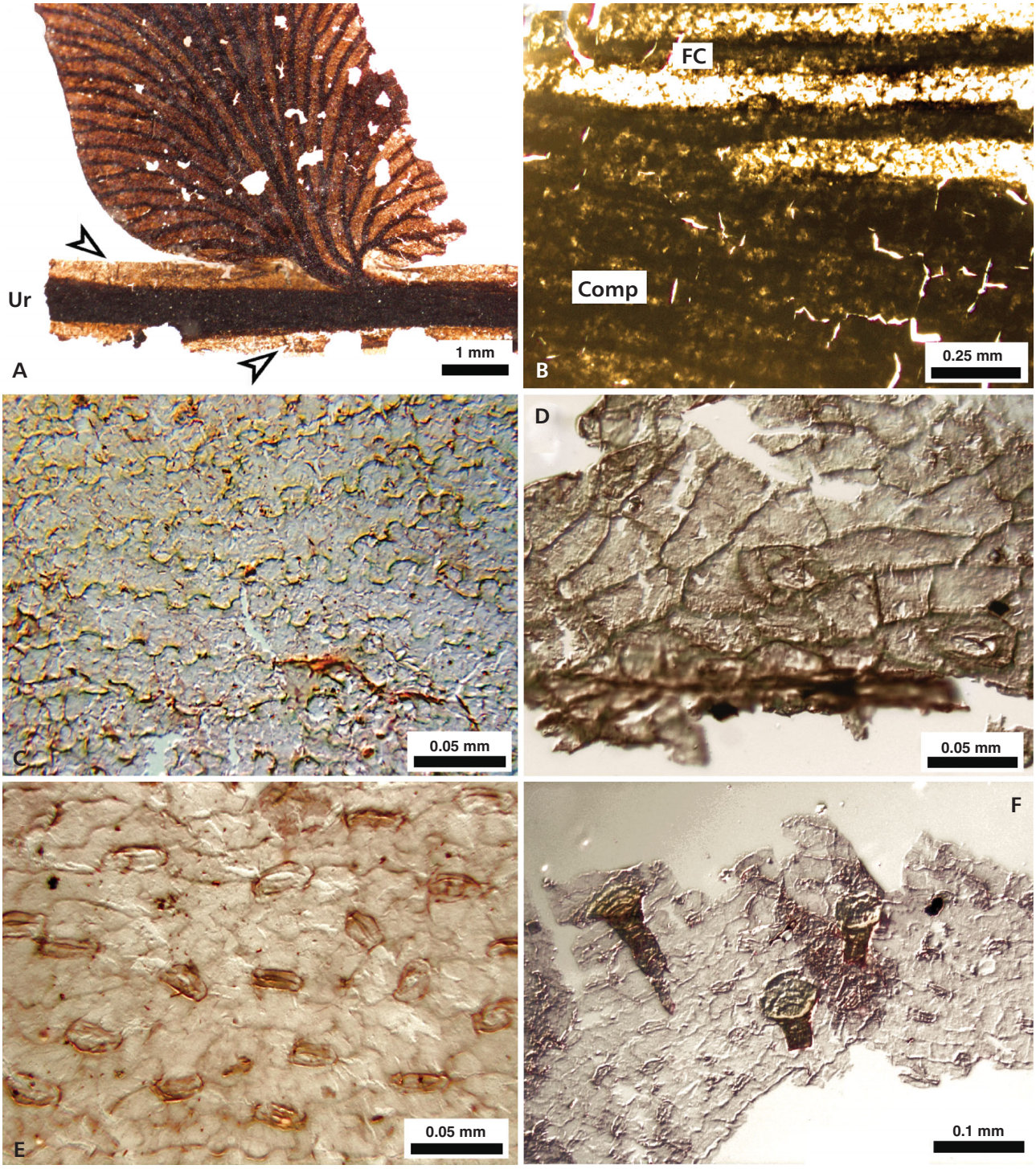

Figure 5. *Neuropteris ovata* var. *simonii*. • A – compression pinnule attached to an Ur, where non-truncated trichomes/files in life position (arrowed) are attached abaxially. HF treatment only. • B – preservation variability in one pinnule, where FC signifies the more naturally macerated part of the compression Comp. HF liberated. • C – sinusoidal anticlinal walls, adaxial cuticle. • D – thicker abaxial cuticle showing curvilinear (intercostal) cells. • E – abaxial cuticle with five or six? anomocytic stomatal rows in the intercostal fields, more or less paralleling the costal fields. • F – internal abaxial surface with ringed trichomatous bases and *ca* six stomatal rows. Nomarski phase-contrast condition, except A, which was photographed in water. Slide documentation: 4Pi 85-248/1; 4Pi 85-248/1; Pi 85-248/2 01; Pi 85-248/2A 02; 4Pi 85-248/7; 4Pi 85-248/2A 04, respectively.

a scientifically parsimonious explanation, or Ockham's razor. The scores reveal information not obvious from the PC plots of the retained loadings. Definitions and interpretations of semi-quantitative IR-derived ratios are given in Table 5 (*cf.* D'Angelo & Zodrow 2011, 2015, 2016).

Fractal dimension. – Mandelbrot (1983) devised the term "fractal" for complex shapes (*e.g.*, clouds, botanical trees) that are not adequately describable by the canons of Euclid, with the connotation of non-integer dimensionality. This research method was formally introduced into palaeobotany by Heggie & Zodrow (1994) in the process of simulating marattialean-frond Aufbau, on the assumption of self-similarity (fractal taxonomy/systematics). Its application to palaeobotany is generally ignored (compare with biology: Smith *et al.* 1996, de Oliveira Plotze *et al.* 2005). The applicability of fractals in palaeobotany is further illustrated here, but codes for derivation and calculation will be presented by Preen *et al*. (unpublished data). We used the "box-counting" method (Minkowski-Bouligand dimension) to obtain the reported fractal dimensions.

Results

Summarized in the first three of the five subsections are micromorphological results. The fourth deals with PCA analysis and chemometric interpretation, and the fifth subsection with fractal dimensions in the framework of cyclopteroid "connectivity" and taxonomic propositions.

Simonii frond, *1–11Pi, 12Pin, compressions*. – Variable opacity and translucency, even in single Pi's (Fig. 5A, B), were observed when submerged in water. Pyrite is present only in trace amounts.

1–11Pi, cuticles. – These are thin but robust, without preserved mesophyll, not easily separable into upper and lower surfaces, except in small fragments <2 mm, and anticlinal walls in intercostal fields of the abaxial cuticles were difficult to track. Consequently, the stomatal index, 30–35, reported by Cleal & Zodrow (1989, table 1), could not be confirmed.

In adaxial surfaces, intercostal fields showed sinusoidal "Ω"- or "U"-shaped anticlinal walls with a fractal dimension of 1.2 (Fig. 5C), and were weakly differentiated from costal fields.

Abaxial surfaces, in contrast, were strongly differentiated between intercostal and costal fields, where the former showed curved and dampened sinusoidal anticlinal walls (*e.g.*, Fig. 5D). Anomocytic stomata, slender, 24–33 μm long and 10–17 μm wide (n = 20), occurred in intercostals fields, and then in large number arranged in four to eight? rows as stomatiferous strips. Polar axes most frequently near-parallel the direction of the costal fields (Fig. 5E), whereas oblique to orthogonal orientation was less frequent. Coastal fields show elongated cells (67–100? μm, n = 3) and narrow (17–30 μm, n = 6), with slightly undulating or with straight anticlinal walls.

Trichomes and bases 47–84 μm long (n = 11) co-occurred with file holes on the intercostal fields (Fig. 5F). Trichomes, however, occurred only in costal fields.

12Pin (Zodrow & Cleal 1988, pl. 2, fig. 1). – Intercalary pinnate structures such as occurring on APUr are referenced in the literature as the form species *Neuropteris triangularis* Bertrand, 1930. Maceration tests yielded only abaxial surfaces. Substituted for descriptive purposes were adaxial surfaces from a detached intercalary specimen 29-237/3 (Table 2) which compared with Pi's of the *simonii* frond in every respect. The fractal dimension is 1.3. Abaxial surfaces of Pin 85-248 (9 slides) and Pi's can hardly be distinguished from one another. We mention that the anomocytic stomata, 27–37 μm long and 7–17 μm wide (n = 18), were distributed in four to eight? rows in the intercostal fields. Trichomatous bases vary in length (40–84 μm, n = 13), and round open structures from 17–37 μm (n = 15), with a distribution pattern as in the Pi's.

Ur 1 and 2. – Compressions are *ca* 2-mm wide, abaxially show trichomes/files (*e.g*. Fig. 4B), are lightly cutinized bilaterally about a much more coalified central-vascular system (*e.g.*, Fig. 5A), likely illustrating differential coalification characteristics. On maceration, a uniform-textured cuticle emerged (*e.g*., Fig. 6A), which on separation yielded surfaces differing in epidermal structures. The surface with near-isodiametric cells (Fig. 6B) showed cells with a range from 24 × 24 μm to 40 × 30 μm, straight anticlinal walls, absences of epicuticular features and stomata, and generally moderate cutinization (compare with Cleal & Zodrow 1989, text-fig. 7D). The surface opposite in Fig. 6C by comparison showed more elongate cells 24 × 14 μm to 44 × 10 μm with straight and cutinized anticlinal walls, and densely (Fig. 6A) but sporadically occurring trichomes in the more central area. Although stomata were not observed in the figured *simonii*-frond specimens, they were nevertheless though rarely, in non-figured specimens, and occurred clustered on a Ur of the *simonii* specimen 82-405 (*cf*. Fig. 11D) that also showed trichomes.

It is instructive to detail further the nature of these elongate cells, with comments on their occurrences in APUr and PUr sample locations. Accordingly, Fig. 6G (detail from Fig. 6C) illustrates the case of a near-isodiametric cell (33 × 27 μm) next to an elongate cell (36 × 25 μm), as is commonly observed in Ur cuticles. The elongate cell appears as a general hexagonal outline, a feature probably ac-

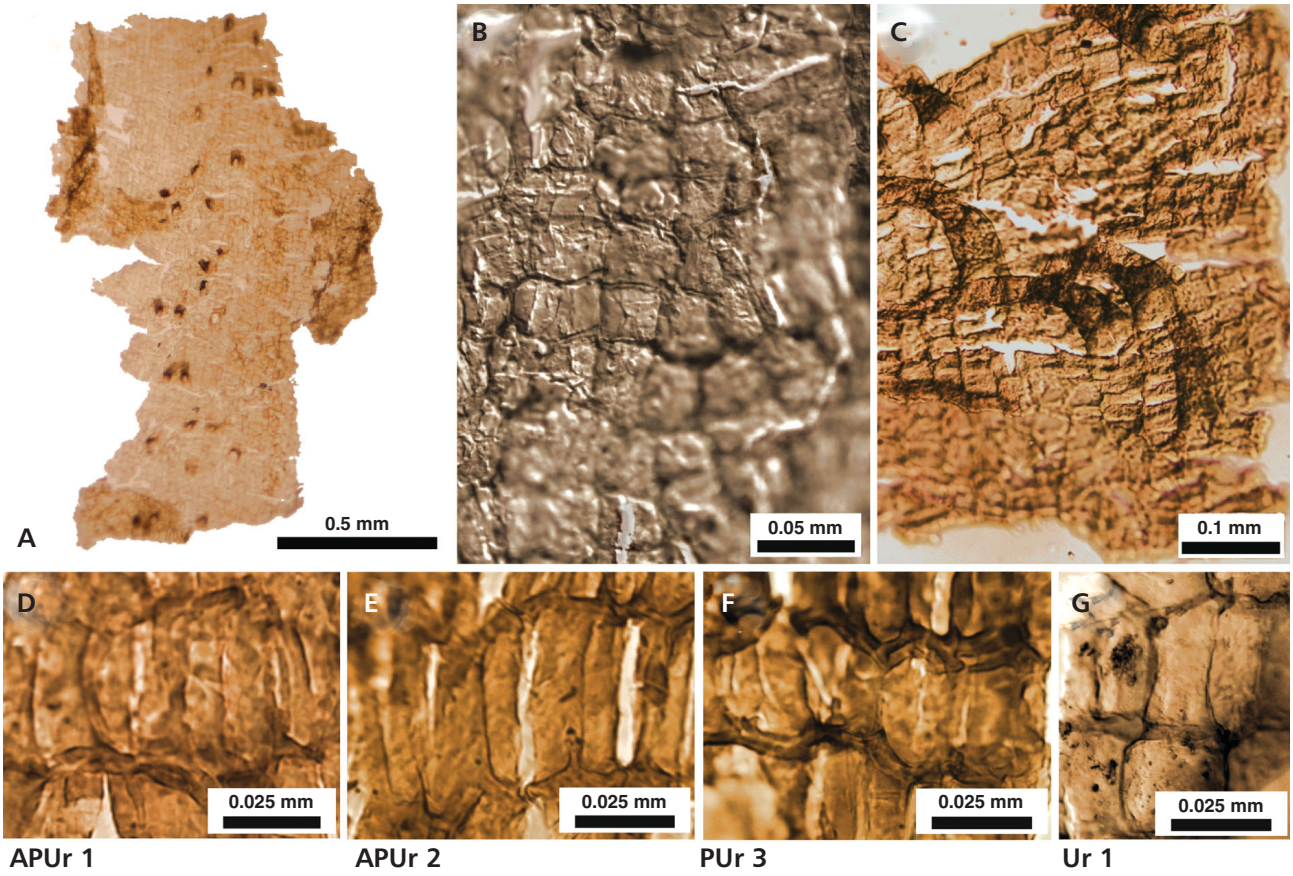

Figure 6. *Simonii* frond Ur 1 cuticles. • A – surface with *ca* 30 truncated trichomes corresponding to C. • B – surface with near-isodiametric cells. • C – surface opposite to B with elongate and near-isodiametric cells, and trichomes. • D–F – examples of elongate cells with "medial" ruptures from APUr 1 and 2 and PUr 3, respectively. • G – detail of C, showing an elongate and a near-isodiametric cell. See the text for explanation. Nomarski phase-contrast condition, except A, which was photographed in water. Slide documentation: Ur 1 85-248/10C; Ur 1 85-248/10A; APUr 1 85-248/12b; APUr 2 85-248/17; PUr 3 85-248/18, respectively.

centuated by the thick cutin, with a distinct straight and thin (not cutinized) "medial line" (taphonomically caused?). The overall appearance is that of a "paired" cell that is, however, prone to rupturing along the "thin medial line", as can be seen in some cells in Fig. 6C. The rupturing effect is particularly well exemplified in cuticles from the APUr's and PUr's (Fig. 6D to F).

PUr 2, 3 and 1. – Compressions are maximally 18 mm wide. The sedimentary infill of the rachis was pyrite-free, but epigenetic micron-sized stringers, or framboidal clusters of pyrite, occurred inside the rachis without being externally visible.

Fig. 7, top to bottom: PUr 2 → 3 → 1, or proximal to distal positions (Fig. 2A) illustrates cuticular similar/differing features on respective surfaces that are summarized as follows. (1) Surfaces with distinct more or less isodiametric cells that are intact and not medially split have consistently been observed (*e.g.* Fig. 7A to C, E), whereas respective surfaces opposite consistently showed the elongate ("paired") cells many of which are split along the "thin medial line" (*e.g.* Fig. 7D; for detail see Fig. 6F). (2) The former surfaces are hardly cutinized and dentate, whereas surfaces opposite are both cutinized and dentate. (3) Trichomes appeared, if at all, at or near the margins of both surfaces and surfaces opposite together with trichomatous (ovate) bases that ranged in length from 50? to 84 µm. (4) File-interpreted structural, open bases 20 to 50 µm (n = 21) occurred on surface opposite (*e.g.* Fig. 7D), though rarely on the other surface (*ca* 20 µm diameter). (5) Rosette-like structures composed of rhomboid cells (*ca* 37 to 43 µm × 20 to 17 µm) quasi encircle smaller structural holes centrally split on the surface (*e.g.* Fig. 7B, arrowed). (6) Only the surface opposite showed stomata (40 × 27 µm), and then very rarely (Fig. 7F).

In terms of dimensions, near-diametric cells are maximally 27 × 20, 33 × 27, and 27 × 23 µm (n = 10/surface), respectively (Fig. 7A, C, E). However, sampling variability is such that a trend direction for dimensions *vs* proximal to distal locations is debatable.

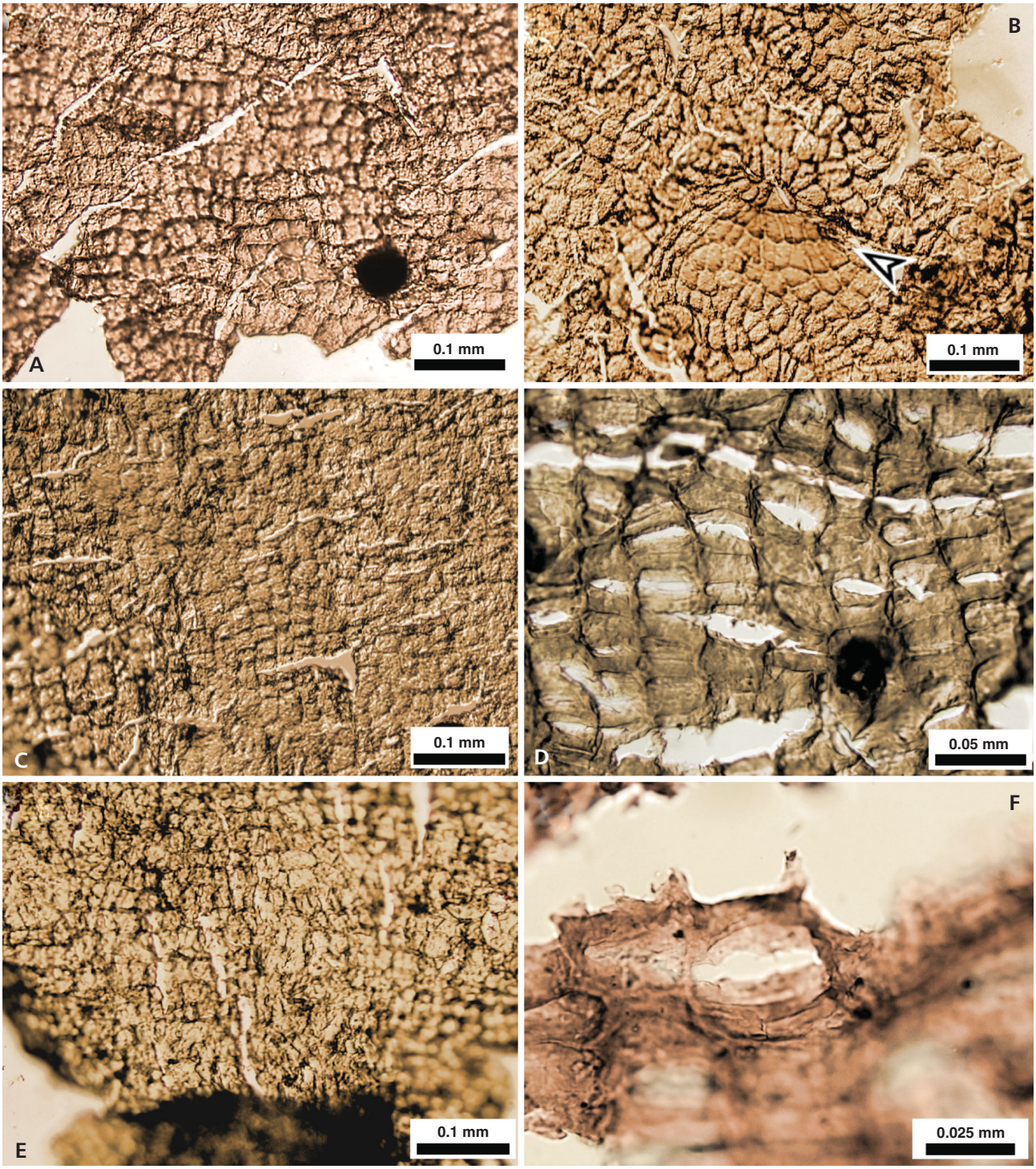

Figure 7. *Simonii* frond PUr 2, 1 and 3 cuticles (proximal to distal: Fig. 2A). • A, B – PUr 2 surface with near-isodiametric cells and rosette structure (arrowed), respectively. • C, D – PUr 3 surface with near-isodiametric cells and surface opposite with elongate cells and a truncated file at lower right, respectively. • E – PUr 1 surface with near-isodiametric cells. • F – a rare stoma on PUr 3. Slide documentation: PUr 2 85-248/11a; PUr 2 85-248/11a rosette; PUr 3 85-248/14; PUr 3 85-248/12; PUr 1 85-248/7; PUr 3 85-248/12 stoma, respectively.

The elongate cells (Fig. 7D) range between 40 × 17 µm to 23 × 10 µm, and conform to comments made under Ur 1 and 2 (see above).

APUr 1 and 2. – Compressions proximally are 15–18 mm wide, tapering to 9 mm distally. The sedimentary infilling was pyrite-free, but epigenetic pyrite was deposited inside the rachial walls.

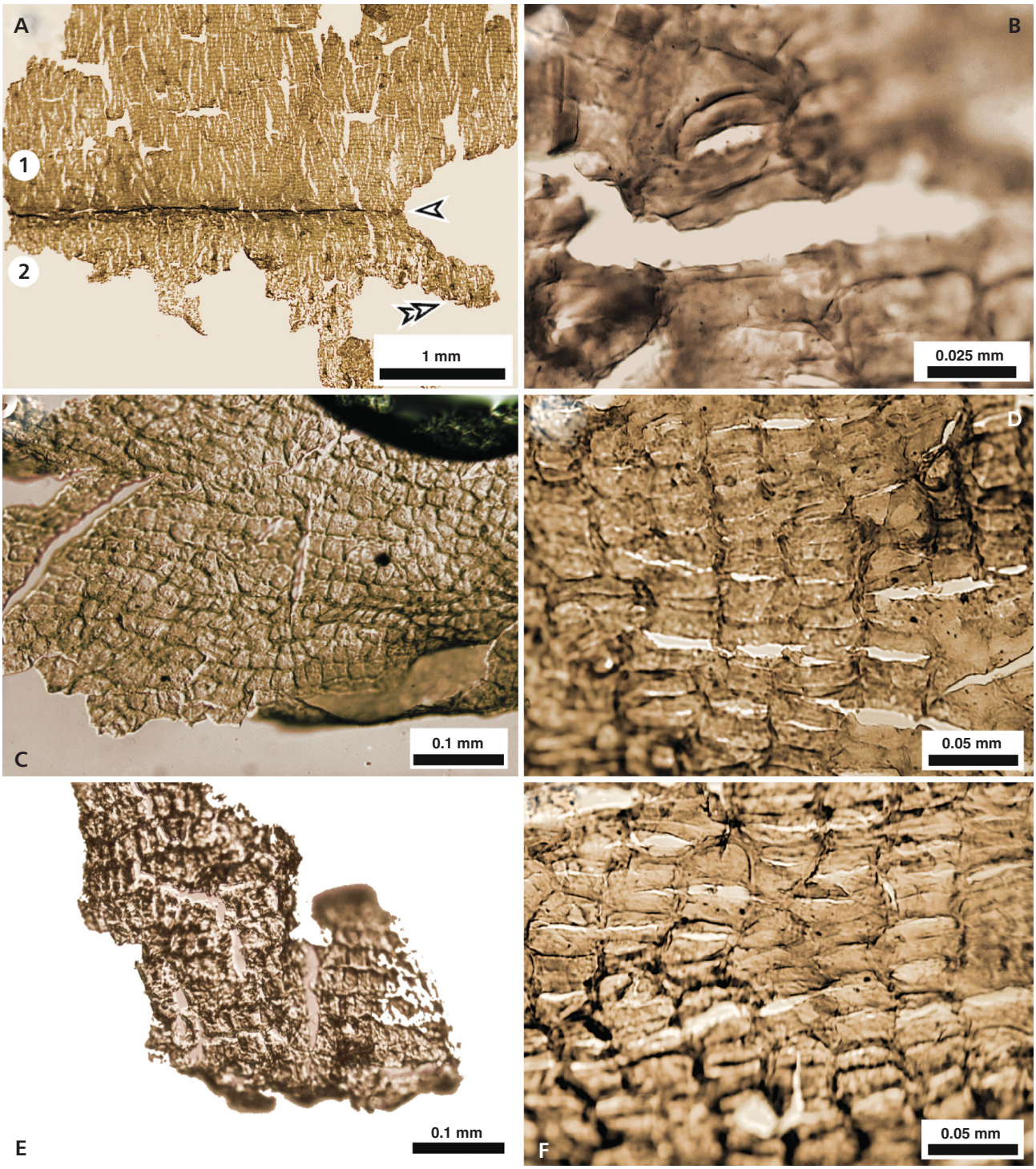

Figure 8. *Simonii* frond APUr 1 and 2 cuticles (proximal to distal: Fig. 2A). • A – APUr 2 showing surface (2) with near-isodiametric cells and surface opposite (1) with elongate cells still marginally attached (arrow). Double arrow points to a file figured in Fig. 3A. • B – APUr 1 rare stoma on a surface with elongate cells (corresponding to (1) in A. • C, D – APUr 1 surface with near-isodiametric cells and surface opposite with elongate cells, respectively. Note secretory organ (black dot) in the former. • E, F – APUr 2 surface with near-isodiametric cells and surface opposite with elongate cells, respectively. Slide documentation: APUr 2 85-248/17; APUr 1 85-248/12; APUr 1 85-248/13 and 85-248/12b new, respectively; APUr 2 85-248/17.

Fig. 8A shows the longest secured, organically connected surface ("2") and surface opposite ("1"), and Fig. 8B a stoma rare for APUr. Similarly to PUr, APUr consists of surfaces with differing epidermal structures. Fig. 8C, E illustrate for APUr 1 and 2 (proximal to distal positions) two respective surfaces with near-diametric

cells, to which correspond the respective two opposite surfaces Fig. 8D, F with the elongate cells. Differences/similarities between the two surfaces are summarized as follows. (1) Near-isodiametric cells of the two surfaces are intact, not medially split, and only slightly cutinized, whereas cells of the two surfaces opposite are highly cutinized with dentate structures and frequently medially split. (2) Trichomes were not observed on either surface of the specimens. (3) Files were mostly truncated, occurring irregularly in clusters on either surface, and open (rarely closed) structural bases (20–50 μm in diameter, n = 46) were noted. (4) Rare rosette-like structures occurred on the surface opposite (slide APUr 1 85-248/12).

In terms of dimensions, proximally the near isodiametric cells range from 17 × 17 μm to 27 × 24 μm (n = 3) (Fig. 8C), and distally from 23 × 23 μm to 33 × 27 μm (n = 6) (Fig. 8E), *i.e*., a slight increase in size? The elongate cells range proximally from 33 × 20 μm to 43 × 27 μm (Fig. D), and distally from 33 × 20 μm to 47 × 20 μm (Fig. 8F). Respective details are shown in Fig. 6D and E. Near the margin, the cells tended to be smaller and near isodiametric (*ca* 20 × 13 μm).

52Ad. – This sample represents the lowest portion of an antepenultimate rachis at, or slightly above, the basal dichotomy (Fig. 2B). Compressions showed no appendages. The cuticles are thin and could not be teased apart, but the two surfaces are clearly visible at an edge and marked "1" and "2", where the cells are of comparable dimensions (Fig. 9A). Specifically, no particular shape is dominant on either surface, but the habit of both hypodermal structures is isodiametric/rectangular. Surface "1" shows cellular dimensions in the range 30–50 μm × 24–36 μm (n = 5), and surface "2" 27–73 μm × 27–40 μm (n = 5); anticlinal walls are straight, not cutinized nor dentate, and trichomes/files and structural holes were not observed.

Pt and its organically attached/associated appendages: (1) to (3). – 51Pt, 48–50Pt represent sample locations in the *ca* 20-cm long petiole (Fig. 2B). The compressions showed no trichomes/files, but cuticles consistently protruded from the edges. With progressing maceration, "chunks" of coal peeled off thereby fully exposing the cuticle. Infill is absent but fine-grained pyrite was deposited.

The cuticles are thin with slightly curved anticlinal walls that appeared diffused, and cellular lengths could not be determined accurately (51Pt was entirely used for FTIR, Table 1). 48–50Pt cuticles are similar in respect to elongate-rectangular and near isodiametric cells (*ca* 40 × 37 μm, 30 × 30 μm, respectively) (Fig. 9B and C). Cutinization and dentate features, trichomes/files, or their corresponding structural holes, and stomatal structures were absent from the samples.

(1) Cyclopteroid leaflet "e" (Figs 2B, 9D to F): The *ca* 2 cm long and 1.5 cm wide preserved pinnule is demonstrably organically connected with the Pt (arrowed in Fig. 9D). Evidence for marginal fimbriae is absent, and therefore an entire pinnule margin is assumed. The fan-shaped venation pattern emanated from a common, smaller area near its stalk-like attachment, which, together with its size, is supportive of a mid-vein-less cyclopteroid-leaflet morphology. Micromorphological information was obtained from the millimeter-sized intact compression lamina (marked "X" in Fig. 9D).

Two cuticular surfaces are evident one of which is thin and epidermally featureless as an assumed adaxial surface. The other is figured (Fig. 9E, F) as being the abaxial surface by virtue of (i) anomocytic stomata (23–37 μm long and 6–20 μm wide, n = 12), (ii) both oval (*ca* 68 μm long, and open, round 17–30 μm diameter) structural holes, and (iii) moderate undulate anticlinal walls, where cells are *ca* 67 μm long, and 26–50 μm wide.

(2) Axis "c" (Fig. 2B "c"): The *ca* 90 mm long and 2.5 mm wide axis, judging from its oriented position, was probably connected to Pt, but all coalified material was eroded. Evidence for any attached structure is an only remaining stalk impression *ca* 2 mm wide, located 2.5 cm from the Pt. From the mm-sized fragments of a closely associated compressed pinnule opposite the 2-mm stalk, corroded pieces of cuticle (8 slides) showed no stomatal evidence, but dense distribution of structural ovate holes, undulating costal cells, and occasional sinusoidal walls, which, when taken as a whole point to *N. ovata* affinity (see Zodrow & Cleal 1988, pl. 4, fig. 1).

(3) Cyclopteroid leaflet "d" (Fig. 2B "d"): Preserved over an area of 2 cm by 1.5 cm was a fan-shaped venation pattern that presumably extended as a fimbriate margin in an intact leaflet. Assumed organically connected and situated basally on the Pt (in close proximity to the Tk), the leaflet base is hidden under the Pt and could not be uncovered for confirmation. Macerating a number of fragments did not show any recognizable cuticular features.

29-31Tk. – The parallel-marked compressed trunk is preserved for a length of 10 cm and a width of 4 cm and assumed organically connected with the Pt, which could not be demonstrated. The *ca* 2-mm thick remains reflect its geochemical/sedimentary-preservation history (taphonomy) (Fig. 10A), which includes the incorporated detrital quartz lenses (*e.g*. Fig. 10B). Moreover, repeated HF treatments indubitably established the presence of rodlets in Tk (Zodrow *et al*., unpublished data), which are interpreted as structural support in medullosalean stems (Lyons *et al*. 1982, and references therein; Zodrow *et al.* 2010).

Cuticles with long and slender cells presumably reflect

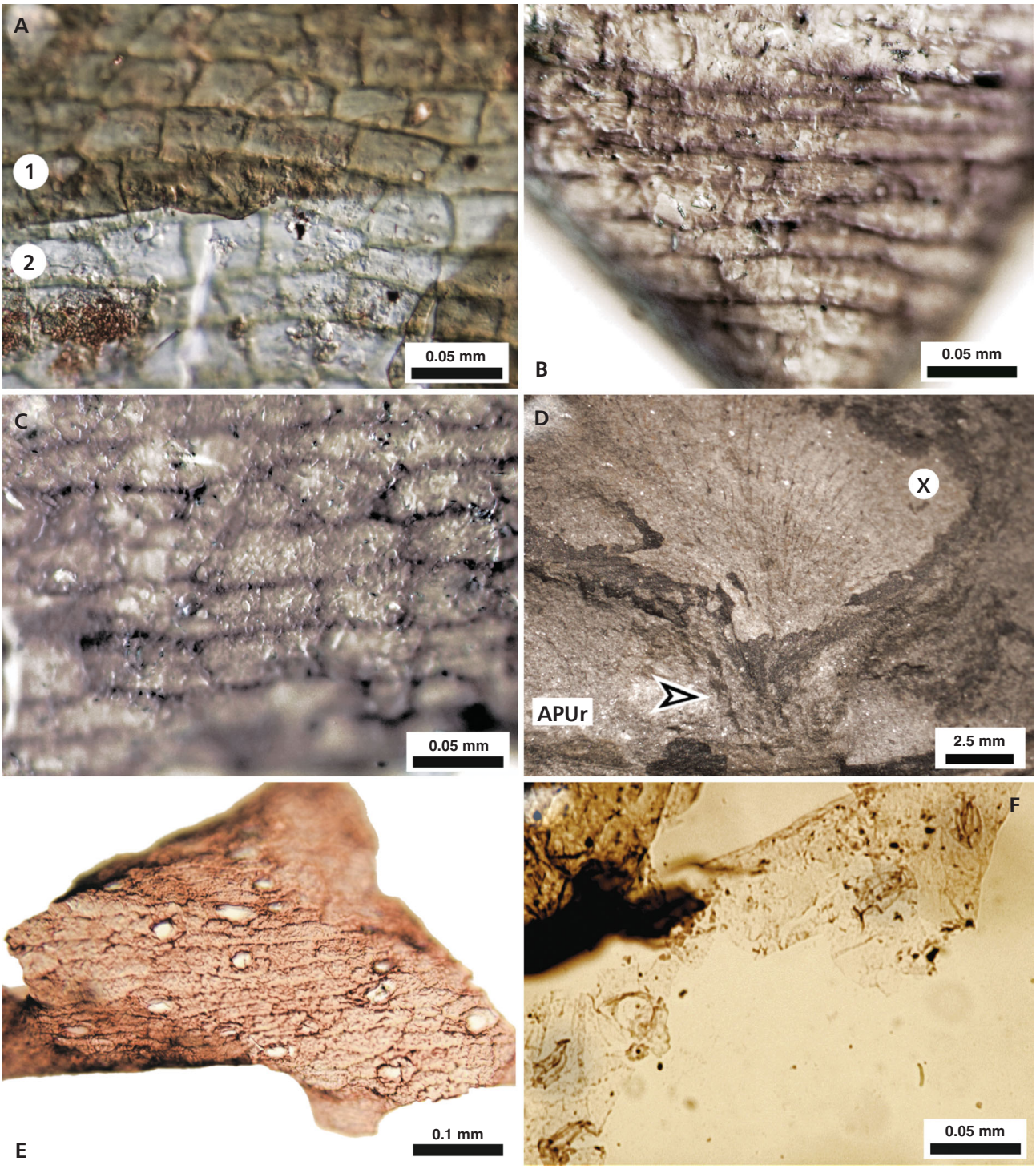

Figure 9. 52Ad, 48-50Pt, and attached cyclopteroid leaflet "e" cuticles (Fig. 2B). • A – 52Ad. Inseparable cuticle but surfaces "1" and "2" are identified. • B, C – 48-50Pt, respectively represent both surfaces of the lower part of the petiole, respectively. • D – "e", cyclopteroid pinnule attached to APUr. "X", location of the macerated cuticle, and arrow identifies stalk connection with the APUr. • E, F – "e", abaxial cuticles with structural holes in the former, and anomocytic stomata in the latter that are preserved in two rows. Nomarski phase-contrast condition, except D, which is by macrophotography. Slide documentation: 52Ad 85-246/2-1b; 48–50Pt 85-246/2 "1" and "2"; 85-246-e 02; 85-246-e2/2; 85-246-e2/3, respectively.

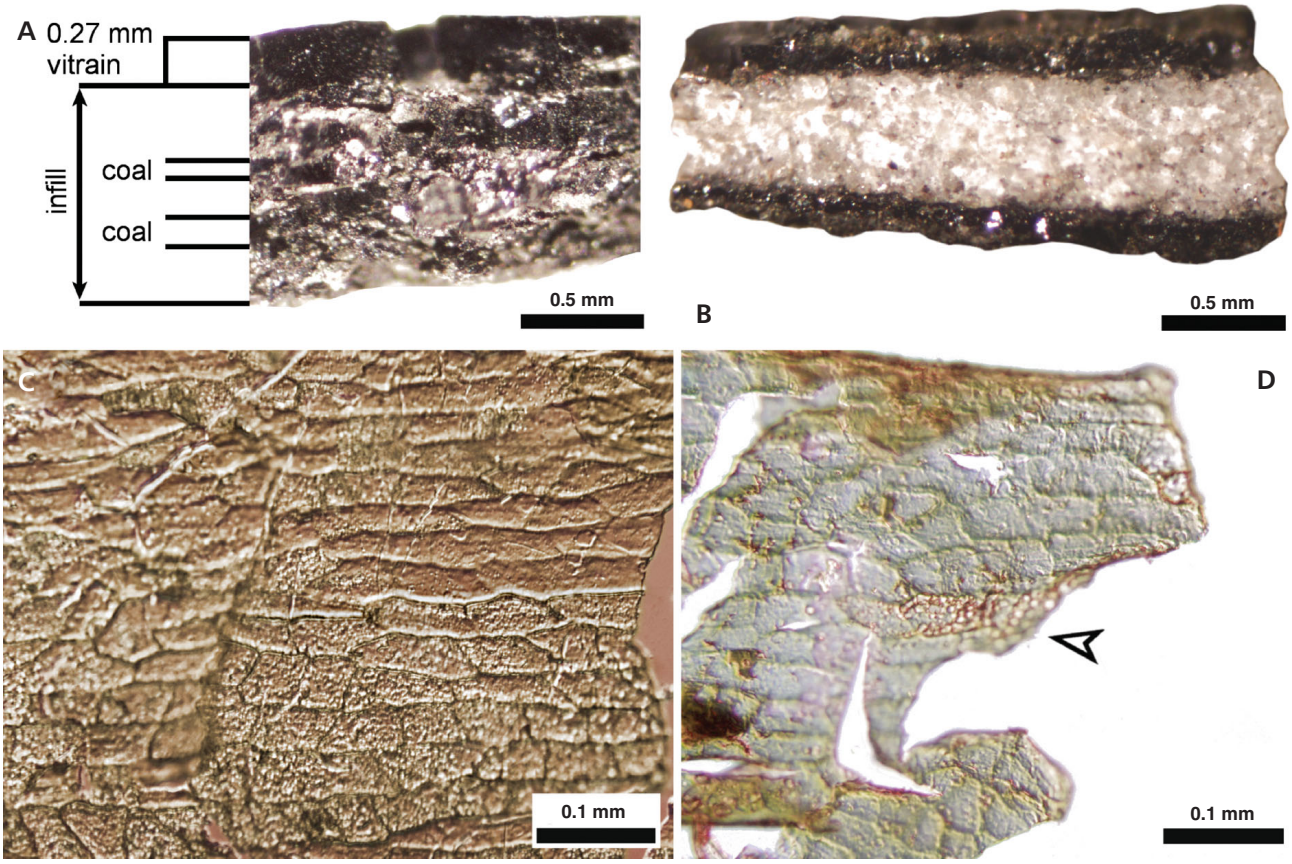

Figure 10. Tk infill and cuticles. Medullosalean trunk associated with the *simonii* frond. • A – less than 50% of the *ca* 2 mm thick trunk "compression" with infill. • B – a clastic quartz lens as part of the infill. • C, D – positions are uncertain in the trunk compression. Arrow in D points to positions (mold) formerly occupied by framboidal pyrite. Nomarski phase-contrast condition. Slide documentation: Temporary slide; Tk 85-246 Quartz vein 3; 29–31Tk 85-246/2; 29–31Tk 85-246/2, respectively.

cortical tissue next to the shorter rectangular ones (Fig. 10C). Length of the former is well over 130 µm, but as delimiting cross walls were not clearly preserved, accurate length measurements were not possible. Width varied between 20–23 µm. The other surface (Fig. 10D) showed shorter rectangular, isodiametric, or rhomboid cells that are 66 × 30 µm to 50 × 40 µm in size, with anticlinal walls generally slightly wavy. Reported are rare stomata, where one is 40 µm long and 17 µm across (not illustrated, slide Tk 85-246-3/5 02).

The depository locations of framboidal pyrite, removed by maceration chemistry (*cf.* Brown 1960), are marked by a cluster of tiny bright points (false color representation).

Simonii specimens. – 32Pi 79-230: For a description see Cleal & Zodrow (1989, pl. 99, figs 3, 4, text-fig. 7D).

33–35Pi 82-405 and 39–41Pi 07-6/15-5a (Table 1). – The compressed pinnule morphology of these two specimens compared with *N. ovata s.l.*, and the cuticular morphology with *N. ovata* var. *simonii* (*cf.* Cleal & Zodrow 1989, pl. 99, fig. 2). Summarized, confirmatory evidence supporting the taxonomic determinations are that the differentiated intercostal fields in abaxial surfaces (Fig. 11A, E, respectively) show (1) anomocytic stomata, 16–33 µm long and 7–16 µm wide (n = 13), arranged into four to seven? rows (Fig. 11B and C, E, F, respectively), (2) a few truncated *in situ* trichomes, co-occurring trichomatous bases 37–97 µm long (*e.g.* Fig. 11C), (3) open structural bases (17–40 µm in diameter), and (4) rare closed structural holes (17–40 µm, n = 3).

The mesophyllous preservation of specimen 07-6/15-5a is documented in Supplementary materials, and figured in Fig. 11E. Ur Epidermal data for the two specimens are summarized in Table 6.

Long ultimate pinna 92-243. – This coalified, fragmentary specimen (Table 2) without preserved tip and base is uncommonly long for its 16 cm (Fig. 12A; *cf.* Bell 1938, pl. 52, fig. 4). The stalked pinnules are auriculate, where the longest is over 19 mm and 8 mm wide, with fan-shaped lateral venation after 1/3 the pinnule length (Fig. 12B).

Adaxial cuticles were differentiated between intercostal (sinusoidal) and costal fields (elongate cells with sinusoidal walls), Fig. 12C. The fractal dimension is 1.2.

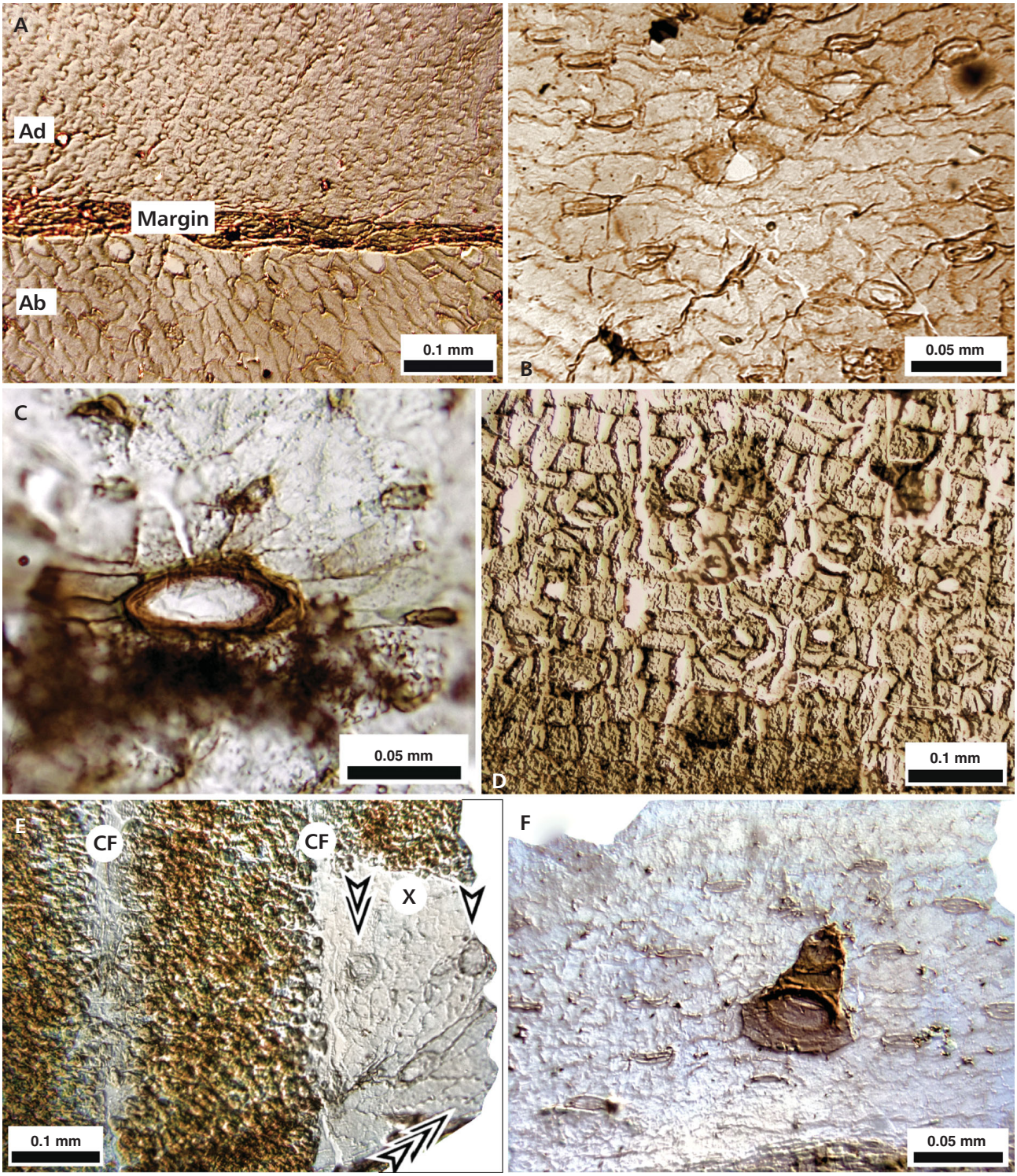

Figure 11. Detached *simonii* specimens 82-405 and 07-6/15-5a, cuticles. • A – 82-405. Ad- and abaxial surfaces still connected. • B – 82-405. Abaxial surface with anomocytic stomata in a four-to-five row pattern. • C – 82-405. Abaxial surface with a "ringed", oval structural base straddling an entire costal field. • D – 82-405. Ur opposite surface with clustered (*ca* 10) anomocytic stomata. • E – 39–41Pi 07-6/15-5a. Two costal fields (CF) between three mesophyllous-covered (brown) intercostal fields. "X" marks an abaxial-adaxial area with stomata, oval-shaped structures (one is arrowed), and an open structural hole (double arrow). The triple-arrow points to the adaxial surface. • F – 07-6/15-5a. Abaxial surface with five or six? anomocytic stomatal rows, and a toppled, truncated stray trichome. Nomarski phase-contrast condition. Slide documentation: 36–38Pi 82-405/2; 82-405/2 stomata; 82-405/5; Ur 82-405/5; 07-6/15-5a/9; 07-6/15-5a/9, respectively.

Table 6. Comparative hypodermal structures of ultimate rachides of *N. ovata*. n.d. – no data

Slide identification	Figure	Surface near-isodiametric cells µm × µm (n)	Figure	Surface opposite elongate (paired cells) µm × µm (n)	Intact cells
Ur 85-248	6B	24 × 24 to 40 × 30 (13)	6C	24 × 14 to 44 × 10 (8)	Yes
Ur 82-405	11D	30 × 30 to 47 × 37 (8)	11D	33 × 20 to 63 × 20 (10)	Yes
Ur 07-6/15-5a	n.d.	30 × 30 to 57 × 27 (7)	n.d.	n.d.	Yes
Ur 92-243	12	23 × 20 to 57 × 27 (6)	12	30 × 17 to 50 × 17 (22)	Yes
Trichomes are prone to occur on either surface.					

Abaxial surfaces were differentiated between stomatiferous intercostal and astomatiferous costal fields. Cellular shapes of both fields, and the anomocytic stomata (14–30 µm long, and 3–16 µm wide, n = 33), in four or five rows (*e.g.* Fig. 12D), compared with the *simonii* frond. Sparingly present are round structural holes (*ca* 17–30 µm in diameter, n = 2), and trichomatous bases 33–47 µm long (n = 13). Mesophyll was not preserved.

The Ur cuticle is *ca* 2 mm wide and separated into the surface with near-isodiametric cells, and the surface opposite with more elongate cells, trichomes, and possibly with stomata (Table 6). A detached and incomplete trichome is 435 µm long and 34 µm wide with *ca* ten uniserial cells.

Confirmatory evidence for the Ur epidermal morphology documented for the *simonii* frond (see the subsection Ur 1 and 2), is summarized by the three Ur's of the *simonii* specimens 82-405, 07-15/6-5a, and 92-243 (Table 6).

Detached cyclopteroid leaflets, compressions and cuticles. – 42–44Co *Cyclopteris* sp. A (82-405, Table 1): The compression was 3 cm across, and probably stalked.

Adaxial cuticles, hardly differentiated between costal and intercostal fields with the inner surfaces frequently covered by mesophyllous material, consisted of polygonal cells (50 × 40 µm to 90 × 40 µm, n = 8) with straight to slightly curved anticlinal walls, and absences of trichomes and stomata (Fig. 13A).

Abaxial cuticles were strongly differentiated between intercostal and costal fields. Intercostal fields showed large near-isodiametric to rectangular cells (40 × 30 µm to 70 × 47 µm, n = 6) with straight or slightly curved anticlinal walls (Fig. 13B). Cutinized anomocytic stomata (Fig. 13B, detail Fig. 15C), occurred in rows of six to seven? in intercostal fields, vary in length 20 to 30 µm and in width 7 to 17 µm (n = 39). Polar axes were mostly parallel to costal fields (Fig. 13C, D). "Star-shaped" open holes are abundant, 20–34 µm in diameter (n = 28), and located at corners of cells in intercostal fields, noting that files, truncated or otherwise, have not been observed. Distributed intercostally and costally were large trichomatous bases that are 57–104 µm long (n = 26), where a base may occupy the entire width of the costal field (*e.g.*, Fig. 13D).

Costal fields, total width of 50–134 µm, showed 2–3 elongate-rectangular cells, 33 × 50 µm to 44 × 233 µm in size (n = 4). The anticlinal walls are slightly curved.

A stalk-like feature, *ca* 660 µm wide, showed isodiametric (*ca* 57 × 57 µm) and rectangular cells (*ca* 37 × 60 µm to 33 × 77 µm, n = 12; Fig. 13E). Stomata were observed located near the margin. Evidence for trichomes and files was absent.

Fimbriate-margined specimens (1), (2) and (3). – (1) *Cyclopteris fimbriata* (82-405C.fim2): This naturally macerated specimen co-occurred with the coalified specimen *Cyclopteris* sp. A (see before) on a bedding plane 2–3 mm beneath the *N. ovata* var. *simonii* specimen 82-405 (Cleal & Zodrow 1989, pl. 98, fig. 2). The specimen was 4–5 cm long, *ca* 2 cm wide (Fig. 14A). Only millimeter-sized fragments of the lamina could be saved of which the fimbriate-vein extensions in Fig. 14B corroborated its state of being naturally macerated. They are interpreted as being abaxial, but confirmatory evidence (stomata) is wanting since maceration caused total destruction of all compression fragments treated. Laminae tend to be narrow (*ca* 85 µm), whereas veins are twice as wide (*ca* 160 µm). Truncated trichomes/files were very abundant on the fimbriae, veins, and on the laminae. Files with parallel base margins were *ca* 150 µm long and 17 µm wide. Laminae without trichomes showed isodiametric (*ca* 33 × 33 µm) and elongate rectangular cells (*ca* 56 × 15 µm), mostly with straight, crinkly cellular walls (slides 82-405C.fim2/3, 4 and 5).

Cuticles from the remaining *ca* 3-mm long coalified rachis (Fig. 14A: marked "Ur") self-separated and fragmented during maceration. Very thin and comparatively thicker cuticles were recovered (Fig. 14C, D, respectively). At least twenty thin (200–400 µm long) and two thicker fragments, 2,000–2,500 µm long, were collected, where in the latter isodiametric-cell dimensions predominated. Only one stoma was found on a thicker cuticle (slide 82-405C.fim2/00). Features common to both surfaces included densely distributed, open, round structural holes (nearest neighbor 10 µm), trichomatous bases were rare, and so were closed structural holes (Table 7).

(2) *C. fimbriata* 45–47Cf (77-443, Table 1; Zodrow & Cleal 1988, pl. 4, 3): Completely used up for the FTIR experiments, after securing cuticles. Compres-

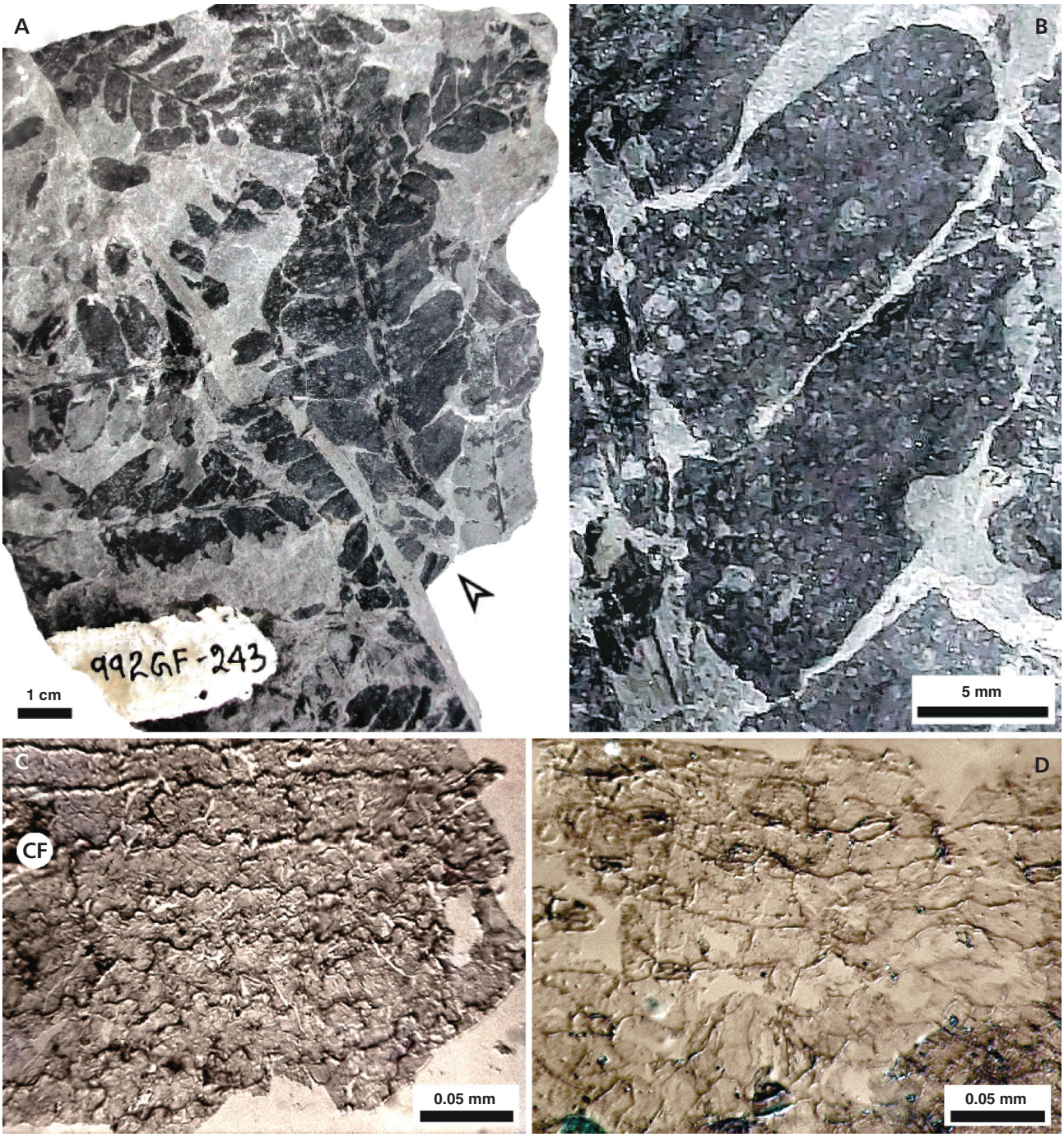

Figure 12. *Neuropteris ovata.* 92-243, cuticles. • A – 16-cm incomplete ultimate pinna, arrowed. • B – auriculate pinnules. • C – adaxial, sinusoidal surface; costal field (CF). • D – abaxial surface with six? rows of anomocytic stomata. • A, B – macrophotography; C, D – Nomarski phase-contrast condition. Slide documentation: 92-243/1 ad; 92-2431b stomata, respectively.

sion fragments from the central part of a pinnule showed differentially coalified/naturally macerated veins over a length of only 4 mm, and laminae that tended to be narrow, *ca* 83–134 µm, compared with 167–200 µm wide veins. Truncated trichomes (maximal length 107 µm), identified by the flared bases, "leaned" across laminae (Fig. 14E).

Cuticles were thin, and the secured fragments impossible to recognize as either ad- or abaxial surfaces. Beeler (1983) pointed out for her coal-ball samples, and before her Gothan (1913) for compressions, that adaxial cuticles were not preserved – but see following cyclopteroid leaflets specimen 92-237. Instead, we rather think in terms of

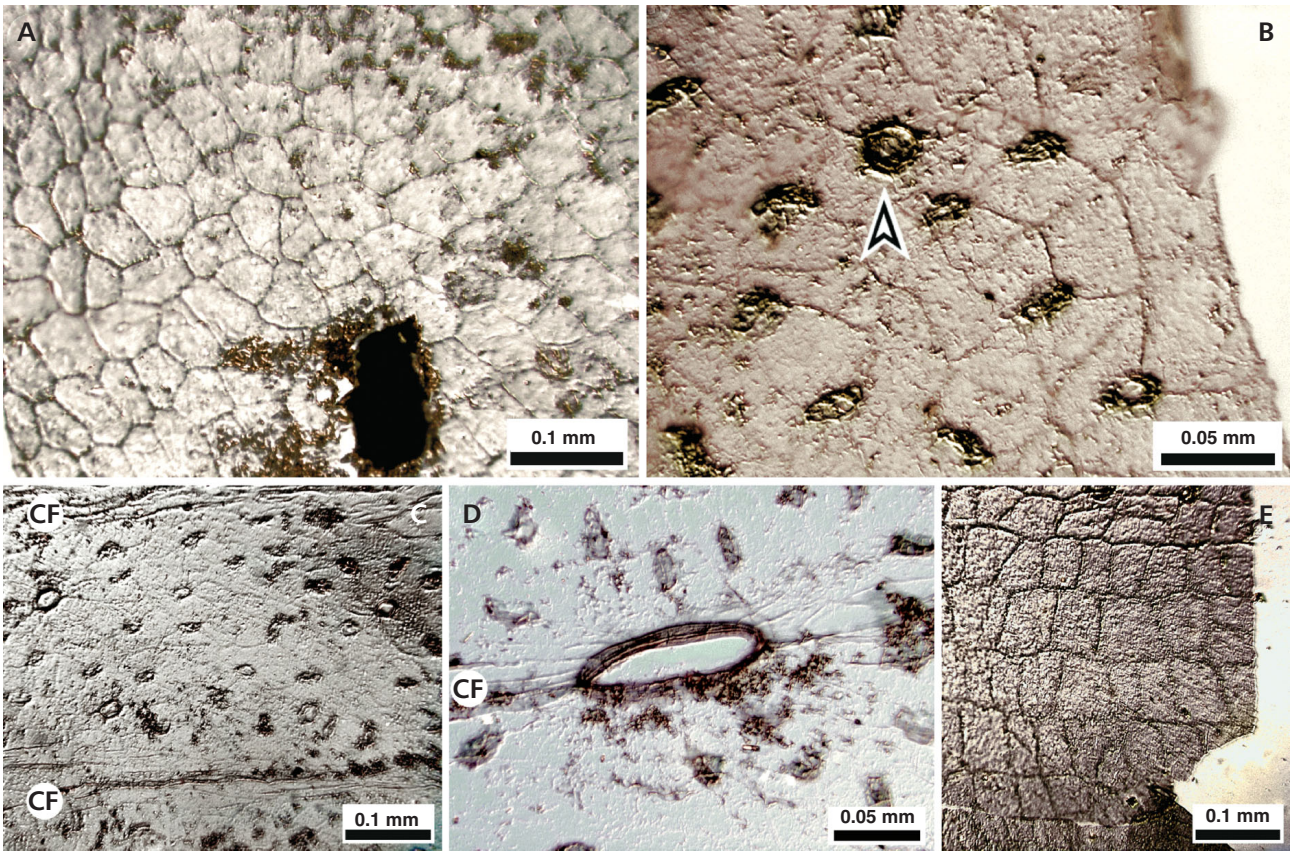

Figure 13. *Cyclopteris* sp. A, 42-44Co, 82-405. • A – adaxial cuticle with polygonal cells. • B – anomocytic stomata and a "star" (arrowed). • C – distribution and orientation of anomocytic stomata (and "stars") in an intercostal field. CF = costal field. • D – ovate structural base straddling an entire width of a CF. • E – near-isodiametric cells from a stalk? "ID" numbers preceding 42–44Co are explained in the text. Nomarski phase-contrast condition. Slide documentation: 42–44Co 82-405/4; 82-405/1b 02; 82-405/5; 82-405/5ringed base; 82-405/3, respectively.

	Structural holes ø		Cellular structure	
	Open, round	Ovate, ringed	Isodiametric	Rectangular
	Range (n)[a]	Range (n)	Range (n)	Range (n)
Thin cuticle	23–44 (24)	33–50 (5)	30 × 36–16 × 36 (9)	33 × 67–10 × 30 (13)
Thick cuticle	16–33 (21)	37–50 (7)	20 × 36–20 × 33 (9)	27 × 40–16 × 23 (7)

Table 7. *C. fimbriata*, 82-405C.fim2 (Fig.14A). Synopsis of epidermal features on thin and thick cuticles of the pinnate rachis. Measurements in µm. Abbreviation: n[a] = No. of samples.

a delicate adaxial surface that was lost, one way or another, during maceration or slide preparation. Anticlinal walls on slides 77-443/5 and 77-443/5a (not shown) suggest a faintly dampened sinusoidal pattern of elongate cells.

Abaxial cuticles showed mostly lengthwise fragmentary fimbriae (Fig. 14F, G) with elongate and narrow cells whose length cannot be determined as dividing walls were eroded; width was 13–27 µm. The anticlinal walls appeared undulate. A single anomocytic stoma was identified as being 27 µm long and 10 µm wide (Fig. 14G, arrowed). Trichomatous bases, 40–70 µm long (n = 12), and round structural holes, *ca* 14–20 µm in diameter were rarely observed.

Figure 14. *Cyclopteris fimbriata*, 82-405C.fim2, 45–47Cf 77-443, and 92-237. • A – 82-405C.fim2, naturally macerated pinnule and rachis. • B – detail of A. HF only. Dense trichome/file population in laminae. • C – Ur 82-405C.fim2, cuticle, thin, with three closely spaced, open structural holes. • D – Ur 82-405C.fim2, cuticle, thicker, with an ovate structural hole (arrowed). • E – 77-443, compression from a central pinnule part with truncated trichomes/files in lumina (L) between veins (V). • F – 77-443, fimbriate cuticle with long rectangular cells and some structural holes. • G – 77-443, fimbriate cuticle with a stoma (arrowed). • H – 92-237, adaxial cuticle. • I – 92-237, abaxial cuticle. Some stomata are arrowed. "ID" numbers preceding 45–47Cf are explained in the text. Nomarski phase-contrast condition, except A, B, and E, which are macrophotographs. Slide documentation: Specimen 82-405C.fim2; Temporary slide 82-405C.fim2; 82-405C.fim2/0 rachis; 82-405/000C.fim2; 45–47Cf 77-443/6; 77-443/1; 77-443/1; 92-237/2A; 92-237/2B, respectively.

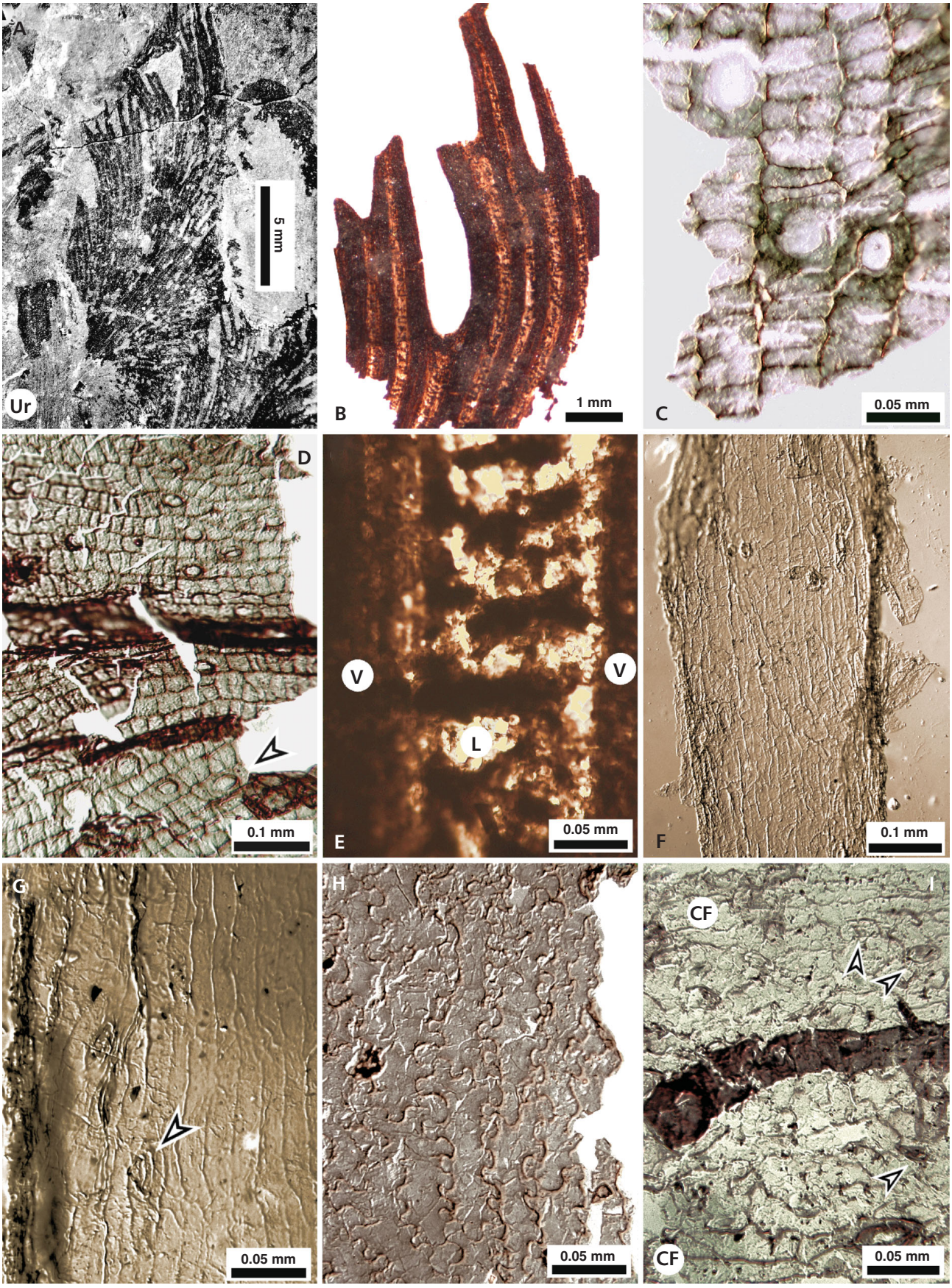
A
5 mm
Ur
B
1 mm
C
0.05 mm
D
0.1 mm
E
V
V
L
0.05 mm
F
0.1 mm
G
0.05 mm
H
0.05 mm
I
CF
CF
0.05 mm

Table 8. Comparative micromorphology of hypostomatal *simonii*-frond pinnules with fimbriate and entire-margined cyclopteroids, and an ultimate *N. ovata* pinna. Abbreviations: [a] Trichomes/files; [b] abundant; [c] sparse; [d] data from re-examining Florin's original slide S010967 (Naturhistoriska Riksmuseet, Stockholm) that after 90 years of storage is in remarkably good condition.

		Adaxial		Abaxial character set					
		Sinusoidal anticlinal walls		Undulate walls		Anomocytic stomata			"hair"[a]
(ID) specimen	Margin (pinnule)	Intercostal (IC)	Costal (C)	IC	C	Rows (IC)	Length (µm)	Width (µm)	Abaxial
(1–11Pi)									
Simonii frond	Entire	Yes	Yes	Yes	Yes	4–6Ab[b]	24–33	10–17	Ab
Intercalary ("*N. triangularis*")	Entire	Yes	Yes	Yes	Yes	4–8?	24–37	7–17	Ab
(42–44Co)									
Cyclopteris sp. A Detached 982-405	Entire	No	No	No	No	6–7Ab	20–33	7–17	Ab
(45-47Cf)									
C. fimbriata Detached 977-443	Fimbriate	Yes?	Yes?	Yes	Yes	?	27	10	Ab
C. fimbriata Detached 992-237/2	Fimbriate	Yes	Yes	Yes	Yes	2–4?	23–26	7–17	Ab
Cyclopteroid "e" Attached 985-246	Entire	Yes?	Yes?	?	?	2?Sp[c]	23–37	6–20	Ab
Cyclopteris sp. (Florin 1925, pl. 10, 3)[d] Detached	Entire	Yes	Yes	Yes	Yes	5–6Ab	17–23	10	Sp
N. ovata pinna Detached 992-243	Entire	Yes	Yes	Yes	Yes	5?	14–30	3–16	Sp

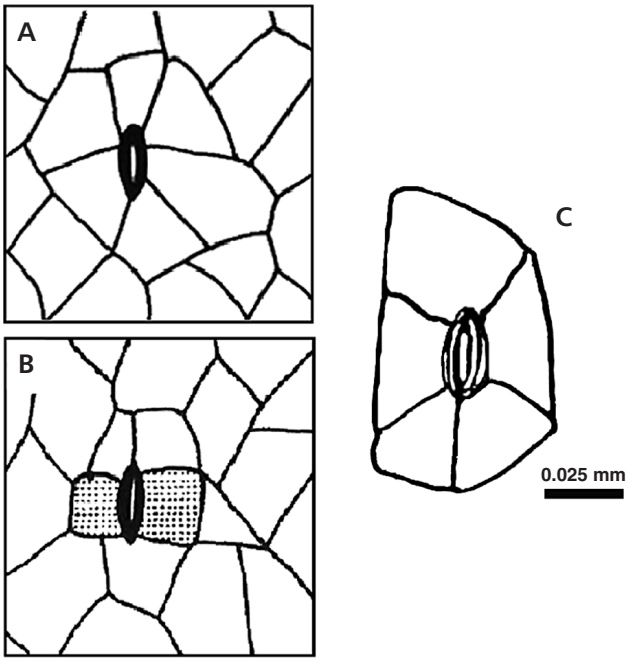

Figure 15. Schematic outlines of anomocytic (A) and brachyparacytic (B) stomatal structures (Cleal & Zodrow 1989, text-fig. 3). • C – anomocytic stoma based on photographs on Fig. 13B.

(3) *C. fimbriata* (92-237: Table 2): Well-preserved adaxial micromorphology, where the fractal-ratio (intercostal/costal) is ~1 (1.26/1.29), Fig. 14H. Intercostal cells were 40–184 µm long and 13–37 µm wide (n = 16), generally linear or slightly curved, and the anticlinal walls were sinusoidal with a variable amplitude. Costal cells are of comparable dimensions but the anticlinal walls were undulatory. Stomata and structural holes of any description were absent from the adaxial surface.

The thinner abaxial surface was differentiated between intercostal (*ca* 200 µm wide) and costal fields (*ca* 50 µm wide), Fig. 14I. Intercostal cells were irregularly polygonal with round termini, 40–68 µm long and 24–34 µm wide, and with undulating anticlinal walls. Stomata (anomocytic type), 23–26 µm long and 7–17 µm wide (n = 16), were rare and occurred in two to four? rows only in intercostal fields, with the polar axis mostly parallel to the direction of the costal cells (Fig. 14I). Costal cells (2–4 per costal field) were long (34–134 µm) and narrow (17–27 µm).

Rare trichomatous bases (40–54 µm long, n = 6) occurred on the costal fields, and trichomes in the intercostal fields, where the figured one is 270 µm long and truncated, and 47 µm wide at the base (Fig. 14I). Files were absent.

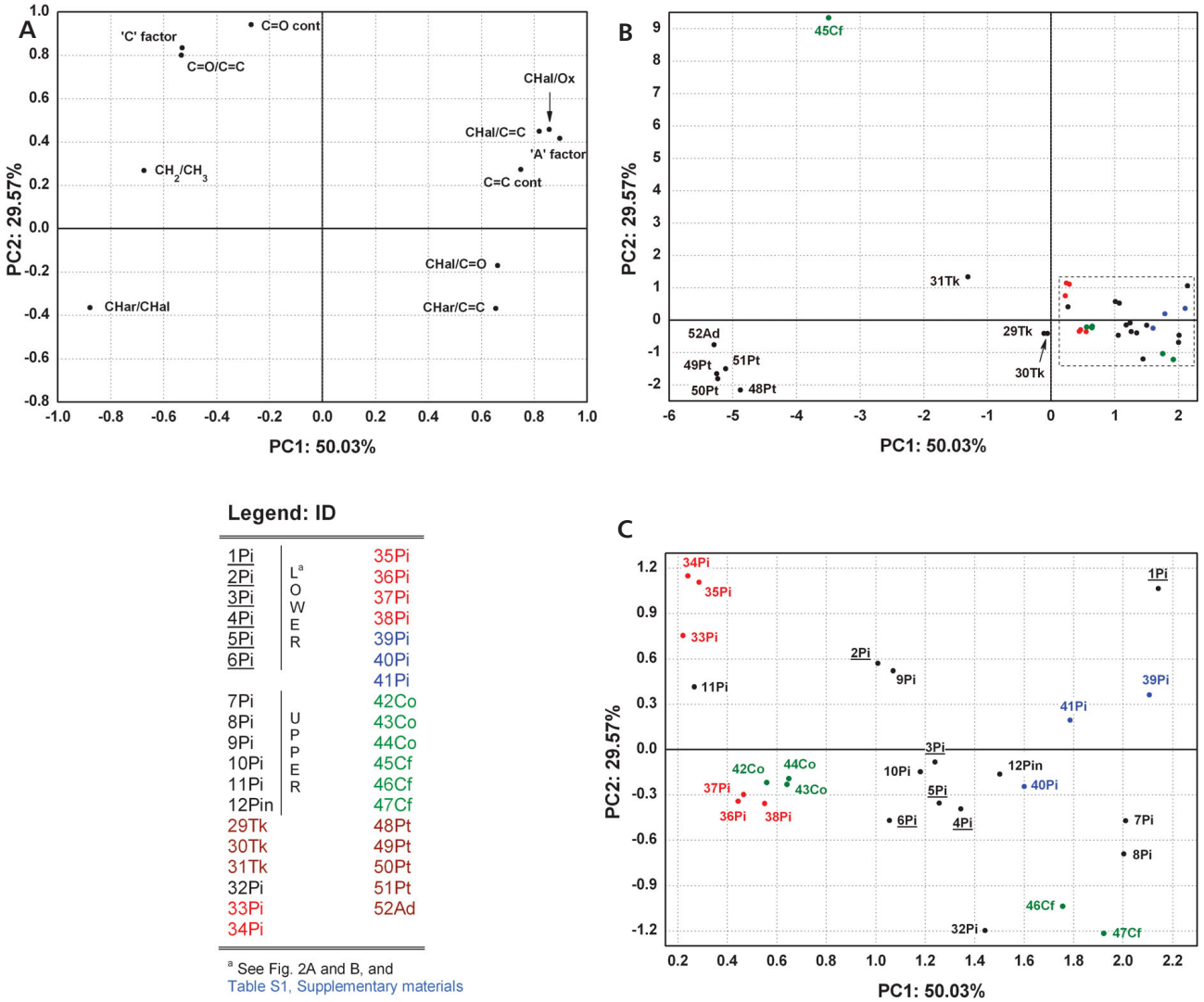

Figure 16. Principal component analysis. • A – plot of PC loadings. • B – plot of PC scores. • C – enlarged plot of blocked area in B.

Table 8 summarizes pertinent data that include those of Florin's cyclopteroid (1925).

PCA and chemometrics. – The IR data and PCA results of the 36 spectra in the analysis, color-coded, and PCA solutions are tabulated in Tables S1 to S4 (see Supplementary materials). Two principal components (PC 1 and PC 2) parsimoniously accounted for 79.6% cumulative variance. Their loading plots and scores are shown in Fig. 16A, B, respectively. The most important component, accounting for the largest variance (50.03%), has positive loadings on "A" factor, CH_{al}/Ox, CH_{al}/C=C, C=C cont, CH_{al}/C=O, and CH_{ar}/C=C, and moderate negative loadings on CH_2/CH_3 and CH_{ar}/CH_{al}. This reflected the complex chemical nature of the samples. Thus, positive loadings indicated mainly the relative abundance of aliphatic functionalities, *i.e.* higher values of "A" factor, CH_{al}/Ox, CH_{al}/C=C, with lower polymeric cross-linking degrees and higher condensation degrees of aromatic rings (*i.e.* higher values of the CH_{al}/C=O and CH_{ar}/C=C ratios, respectively). Moderate negative loadings involved in PC 1 reflected longer methylenic chains (higher values of CH_2/CH_3) attached to less substituted aromatic rings, expressed by higher aromaticity or CH_{ar}/CH_{al} values.

Pinnules, 1–11Pi, 12Pin, 32Pi–41Pi, and cyclopteroid leaflets 42–44Co and 46–47Cf, exhibited the most positive scores against this component (Fig. 16B, C, *x* axis). In effect, this reflected their high contents of aliphatics (highest values of "A" factor) with shorter side chains (lowest CH_2/CH_3 values) attached to benzene rings showing higher degrees of condensation (highest values of CH_{ar}/C=C).

Trunk samples (29-31Tk) showed moderately negative scores against PC 1 (Fig. 16B, *x* axis), indicating similar contents of functional group in comparison with pinnule

Table 9. Fractal dimensions (adaxial surface) of *N. ovata sensu lato*. Abbreviation: [a]Florin (1925, pl. 10, fig. 7).

Specimen	Margin	Fractal dimension	Figure
4Pi *Simonii* frond	Entire	1.2	–
N. ovata pinnule Long ultimate pinna 992-243	Entire	1.2	–
Intercalary Pinna	Entire		14H
Intercostals		1.26	
Costal 992-237		1.29	
Cyclopteris sp.[a] Slide S010967	Entire	1.4	–

specimens. Sample 31Tk showed higher carbonyl contents than the other pinnule and trunk specimens.

Petiolate samples (48Pt-51Pt, and 52Ad) have the most negative scores against PC 1 (Fig. 16B, *x* axis). The latter is the result of the highest aromaticity expressed by the highest CH_{ar}/CH_{al} ratios, along with the lowest condensation degree of benzene rings, or CH_{ar}/C=C values. Such relatively unsubstituted aromatic structures are attached to the longest and least branched polymethylenic chains.

PC 2 (29.57% explained cumulative variance) has very high positive loadings on C=O cont, "C" factor, and C=O/C=C. The latter accounted for the functional groups characterizing naturally oxidized materials. The only fossilized-cuticle specimen (45Cf, *C. fimbriata*) showed the most positive score against PC 2 (Fig. 16B, *y* axis), having the highest cross-linking degrees of the polymeric structures (= the lowest values of CH_{al}/C=O).

A simplified, full-scale plot of PC scores (Fig. 16B) is shown by Fig. 17A. Here, data groupings are depicted in terms of three frond parts *i.e*., trunk, petiole and pinnule. Fig. 17B is the corresponding simplified plot of the boxed area in Fig. 17A showing approximate zones corresponding to upper and lower pinnules, and proposed chemometric *C. fimbriata* and *Cyclopteris* sp. A positions in the *simonii* frond. Ellipses delimiting the groups have no statistical significance.

Fractal dimensions and taxonomy. – We argue that advanced mathematical techniques, when used as part of the descriptive morphology, promote a more objective and consistent taxonomic approach together with systematic applications, than the classic-descriptive morphology by itself. As an example, we introduced fractal dimensions as a quantitative measure of "sinusoidal anticlinal walls", which for the *N. ovata* specimens lie in a narrow sample range from 1.2 to 1.4 (Table 9). Intimated is that the subjective statement "intercostal fields are differentiated from costal fields [adaxial surface]" is objectively replaceable by the quantitative ratio of their respective fractal dimensions. And we used the very narrow range of values of fractal dimensions (statistical implication for one *ovata*-sample population) for an objective measure for connectivity of cyclopteroids with the *simonii* frond (Preen *et al*., unpublished data).

Discussion

Diagenetic-chemical factors

As found in previous studies of Sydney-Coalfield specimens, differences exist in the IR ratios, particularly CH_2/CH_3, CH_{al}/Ox, C=C cont, C=O cont, and CH_{ar}/CH_{al}, between compressions (coalified) and naturally macerated cuticles (fossilized cuticles; Zodrow & Mastalerz 2009) of the same species, from the same sample location. This indicated that on average the hydrocarbon chains of the naturally macerated pinnule 45Cf tend to be longer and have less side branches than the compressions 1–11Pi, 12Pin, 32Pi, 33–38Pi, 39–41Pi, 42–44Co, and 46–47Cf (Supplementary materials, Table S1). Higher carbonyl contents and cross-linking degrees confirm the higher degree of oxidation of 45Cf, relative to the other specimens analyzed.

Consistent with case studies of uneven preservation in compression floras was the experience of obtaining differing cuticular quality from Pi batch to Pi batch, or from differing sample positions, in the *simonii* frond, and from the *simonii* specimens that were comparatively more coalified (*cf*. D'Angelo *et al.* 2012, Zodrow & D'Angelo 2013, D'Angelo & Zodrow 2016).

Micromorphological aspects

The micromorphological features of the entire pinnule set 1–11Pi, 12Pin, 32Pi, 33–38Pi, 39–41Pi of the *simonii* material are similar to those described by Cleal & Zodrow (1989) for *N. ovata* var. *simonii*. The similarity, as opposed to differentiated intercostal from costal fields in the adaxial cuticles, is likely the result of the presence of a hypodermis, which served as a buffer between bundle-sheath extensions and the epidermis (*cf*. Stace 1984). Cleal & Shute (2012) hypothesized that the absence of a hypodermis can be deduced from the difference between intercostal and costal fields. The *caveat* is that the only known permineralized specimen of *N. ovata* does not show hypodermal cells (Beeler 1983).

The size, shape and distribution of the anomocytic stomata in the *simonii* material are position-dependent considering the following. (1) Pinnules are consistently

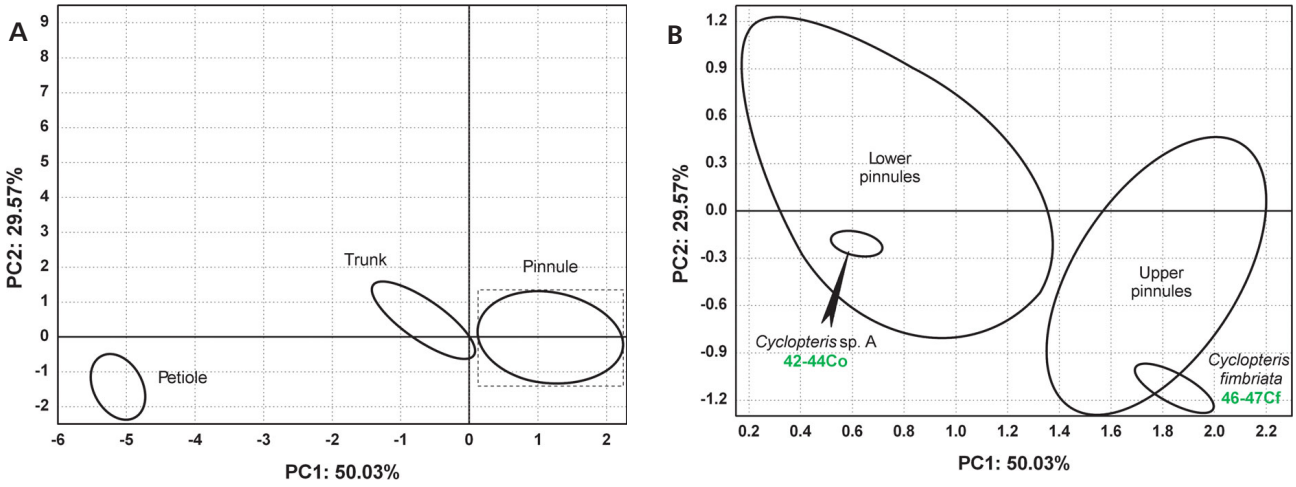

Figure 17. Simplified plots of Fig. 16A, B. • A – full plot indicating data groupings for different frond parts *i.e.*, trunk, petiole and pinnule. • B – detail of the area delimited in A, showing approximate zones corresponding to *N. ovata* var. *simonii*, *C. fimbriata* and *Cyclopteris* sp. A. Fossilized-cuticle specimen 45Cf is excluded for a better visualization. Ellipses in this figure have no statistical meaning.

hypostomatic with long and slender stomata arranged in multiple rows, whereas in the various rachial orders of the *simonii* frond they tend to be sunken, comparatively larger, oval shaped, relatively rare and randomly distributed. Whether they are amphistomatic remains unresolved. Brachyparacytic stomata were not found (see Cleal & Zodrow 1989).

We are in a position to present an outline of the hypodermal structure of the *simonii* frond in terms of a three-fold micromorphology (Fig. 18), from the trunk to the pinnules, as follows, and hypothesize its generality for medullosalean fronds:

(1) Near-isodiametric-rectangular cells with surfaces undifferentiated from surfaces opposite from the trunk upwards to and including the lowermost part of the main frond dichotomy. Cells are non-cutinized and non-dentate. Trichomes/files were not observed.

(2) Near-isodiametric and elongate cells consistently differentiated between the surface and surface opposite for all rachial orders, respectively. Cells are very cutinized and dentate, excepting Ur. Trichomes/files tend to be present in surfaces opposite. Noted are round structural holes of unknown origin(s). The uncertainty about the amphistomatic nature for APUr and PUr precludes designating upper and lower surfaces. However, we have evidence from compressions and cuticles that the surface opposite in Ur's are organically connected with the lower pinnule surface (*e.g.*, Fig. 4B).

As far as we know, the co-occurrence of the intact epidermal structure and the phenomenon of "medial" cellular splitting in the surfaces opposite has not been previously described from medullosalean fronds.

(3) Polygonal cells with gently curved anticlinal walls in the lower pinnule surface are consistently differentiated from sinusoidal cells in upper pinnule surface, including intercalary pinnules and cyclopteroid leaflets.

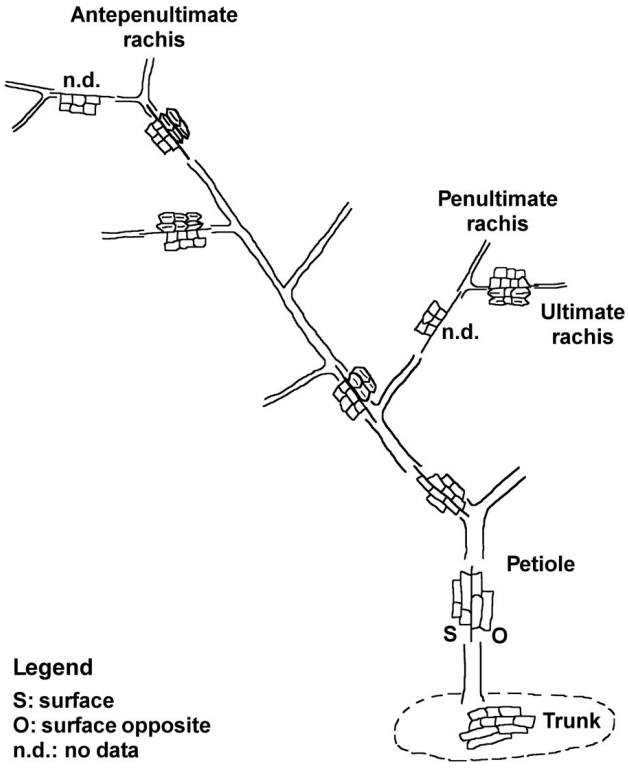

Figure 18. Hypodermal makeup in the *simonii* frond from the trunk to an ultimate rachis proposed as a model for medullosalean fronds. Not to scale.

Organic attachment of cyclopteroid leaflets of entire-margined "e" and fimbriate-margined "d", and in particular that "e" has *N. ovata* micromorphology, confirm the

Pt specimen (Fig. 2B) as a main bifurcation for *N. ovata* by arguments of homological morphology, already hypothesized by Zodrow & Cleal (1988). We take this one step further, by the compelling evidence of physical association of Pt-Tk (Fig. 2B), and assume them to be *ovata*-frond constituents. Supportive evidence is presented by the chemical data as indicated by our chemometric study (PC model, see later). Furthermore, the epidermal similarity between the "e" cyclopteroid and the *simonii* pinnules leaves little doubt of a homologous relationship in the *ovata* frond (see also Florin 1925). Considering also the presumed attachment of the 9-cm long axis "c" to the Pt fits the macrodescription of the pinnate axes of the compressed unipinnate *C. fimbriata* specimens from Sydney. Thus, the evidence strongly points to an *N. ovata* frond with complex laminate cyclopteroid structures below the main dichotomy.

The detached, round *Cyclopteris* sp. A (42-44Co) found associated with the *N. ovata* var. *simonii,* and also with the *C. fimbriata* (92-237/2) specimens, could *a posteriori* be grouped with *N. ovata* var. *simonii* by Rothwell's (1985) criteria of physically associated organs. But the structure and distribution of the stomata and the abaxial occurrence of the ovate structural bases (Table 8) in *Cyclopteris* sp. A call for a micromorphological comparison with the *Neuropteris ovata* var. *aconiensis* Cleal & Zodrow (1989, pl. 101 and text-figs 11b and 12a to c) (summary: Table 10). This comparison is moreover supported by the weakly differentiated adaxial surfaces of both species, and lack of the structural ovate holes, signaling an absence of trichomes, though cellular dimensions are somewhat larger for the *Cyclopteris* sp. A. Abaxially, the comparison also holds for the intercostal fields with their gently-curved or straight walls, except that the costal width in *N. ovata* var. *aconiensis* is greater (or *ca* 350 μm), and cells less rectangular than in the 134-μm wide costal fields of *Cyclopteris* sp. A. This raises the question of origin, or from what frond, or part thereof, did *N. ovata var. aconiensis* drop off? A discussion of this problem is beyond the scope of the present study.

A far-reaching implication is that entire or fimbriate-margined cyclopteroid leaflets found in physical association with foliage of *N. ovata s.l.* may not necessarily be an organic part of that frond, *e.g.*, Lyons & Laveine (2005). In such situations confirmatory micromorphology combined with chemistry to evaluate connectivity is a prerequisite. In contrast, none of the analyzed detached fimbriate specimens in this study is excluded from being *N. ovata s.l.* on micromorphological grounds.

Brongniart's "round ferns" may thus assume two marginal characteristics insofar as the *ovata* frond is concerned: (i) entire or round, and (ii) fimbriate or fringed (this study). However, the proclivity for abscission (*cf.* Darrah 1969, this study, and others) continues to hinder knowledge of their morphological frond positions (see following).

Chemometric hypotheses

The PC scores (Figs 16 and 17) are clear and supportive of *Cyclopteris* sp. A (42-44Co) being a well-defined group onto itself, different from *C. fimbriata* (46-47Cf), although micromorphologically the latter is of the *ovata* group (*N. ovata* var. *aconiensis*). Chemically, *Cyclopteris* sp. A (42-44Co) is characterized by a higher level of aromaticity, having a comparatively lower condensation degree of aromatic nuclei (benzene rings), whereas *C. fimbriata* (46-47Cf) has a comparatively higher aliphatic contents with lower C=O cont and CH_2/CH_3 values. However, 45Cf must be excluded because it is very different from the other two *C. fimbriata* samples, as it is more of a typical-fossilized cuticle by having higher contents of C=O cont and "C" factor. Chemometric results also showed that 46–47Cf *C. fimbriata* plots closely to the upper part of the *simonii* frond, *i.e.* 7–9Pi, 12Pin (Fig. 17B). The broader implication is that "*C. fimbriata*" may not have been a foliar element occurring exclusively below the main frond bifurcation: it is also hypothesized to have occurred above it in the *N. ovata* frond. But to what level in an APUr remains unresolved. Beeler's (1983, fig. 45) positioning of round cyclopteroids on a main rachis could probably be a guide, but her model was based on coal-ball data from which details of frond architecture are difficult, if not impossible, to establish. On the basis of further chemical experiments, arguments of the likely attachment of *N. ovata* cyclopteroid leaflets to the upper part of the frond will be more fully developed in a future study (D'Angelo & Zodrow, unpublished data). Included will be a discussion on the connectivity among Tk-Pt with APUr.

Furthermore, the PC scores in Fig. 17A, B mimic chemically the tripartite micromorphology of the *simonii* frond as confirmation of our hypothesis of the relationship of the frond Aufbau – architecture and chemistry. Likely chemometric-based implications for biomechanics, paleoecology, and paleophysiology of the *simonii* frond will be addressed in a separate contribution (D'Angelo & Zodrow, unpublished data).

Polymorphism below the main bifurcation

This remains a little more speculative, but we can take any of Laveine's synthetic frond models of *Neuropteris*, and appreciate a trend of polymorphic foliage below the main bifurcation (Laveine 1997, figs 4, 11, 13, 19). The most general trend in the changing segmental morphology, starting proximally at the stem (S) and proceeding distally to the

Table 10. Micromorphological comparison between *Neuropteris ovata* var. *aconiensis* and *Cyclopteris* sp. A, with common anomocytic stomata. Measurements in μm.

Species	Adaxial surface		Abaxial surface			
	Walls	General shape	General shape (size)		Stoma	
	(anticlinal)	(size)	Intercostal	Costal	Length	Width
Cyclopteris sp. A	Straight	Polygonal (50–90)	Polygonal (30 × 70)	Polygonal 33 × 233)	20–33	7–17
N. ovata var. *aconiensis*	Straight	Polygonal (20–60)	Polygonal (20–60)	Polygonal (40–200)	10–20	6

main bifurcation, is depicted as follows and highlighted by color code.

Laveine's synthetic model:

(a) (S) cyclopteroid pinnule → bipinnate → unipinnate segmentation – main frond bifurcation.

Present evidential specimens:

(b) (S) fimbriate pinnule → long axis with unknown foliage → entire-margined cyclopteroid – main frond bifurcation.

A certain degree of congruency between the synthetic model and evidential specimens appears to be the case. However, chemometrics introduced differences for comparisons, which are accommodated by our thinking that even fossil taxa can be described by more than just one set of parameters. An example is *Cyclopteris* sp. A (42-44Co), that although chemically speaking is *N. ovata* var. *simonii*, micromorphologically it is *N. aconiensis*, where the latter is known only from detached pinnate foliage. The chemical-chemical comparison of 1–6Pi pinnules from the lower part of the *simonii* frond with *Cyclopteris* sp. A implies a basal cyclopteroid element to this frond. A different interpretation arises with *C. fimbriata* (46–47Cf), which though micromorphologically identifiable with *N. ovata* var. *simonii*, is chemically comparable with the upper 7–9Pi, 12Pin pinnules of the s*imonii* frond. Such "apparent discrepancies" are mainly due to the different natures of the data involved. Though micromorphology/compression is also used in support of organic connection of physically associated plant remains, IR-derived chemical information constitutes a complete set of data of the entire group of compression-preserved leaf tissues *i.e.*, not just the cuticle. Such holistic information (which includes the cuticular composition) provided by chemistry does not necessarily match other (more limited) taxonomic-derived criteria (*e.g.*, micromorphology) used to define certain aspects related to the reconstruction of disarticulated fossil plants, or their taxonomy/ systematics. Defining the best biological criteria to be considered in obtaining a better and more natural taxonomy of fossil leaves implies the use of the most comprehensive set of characters available. The latter means, for example, that not all of the features now considered reliably useful to achieve a realistic taxial classification should continue to be used. Eventually, some characters should be disregarded because of meaningless or of limited utility. That is the case demonstrated for some foliar characteristics (*e.g.*, epidermal features) of living plants, which are variable along the length of a single leaf lamina (*e.g.*, Miranda *et al.* 1981). Our approach of morphology/micromorphology combined with chemistry therefore presents the alternative to Brongniart's model of morphological taxonomy (*cf.* Stafleu 1966, p. 321).

Autecology

This is also based on the *simonii* frond. The occurrence, however rare, of densely clustered (and of single occurrences) of stomata on Ur is suggestive of a similar situation for PUr and APUr, which together with the stomatiferous pinnule "e" points to photosynthetic capability over the entire frond. Not ruled out is sample bias for the non-observation of stomata on Pt. The dense distribution of trichomes/files can be compared with *Macroneuropteris scheuchzeri* (Zodrow *et al.* 2014). But for both species, and indeed for medullosaleans in general, the function(s) of these features are as yet concretely unknown, unless the analogy with angiosperms holds (Fahn 1979, Khan *et al.* 2015).

Based on a combination of IR-derived data, it is possible to infer some aspects of the autecology of the *simonii* frond (D'Angelo & Zodrow, unpublished data). The functional groups detected are related to diagenetically resistant molecules, *e.g.*, lignin-, tannin-, resin-like polymeric structures, and others? The presence of lignin units in the fossil record is chemically somewhat difficult to demonstrate, requiring the detection of (di)methoxyphenols with attached side chains. The presence of benzenediols and phenols without attached side chains indicates likely condensed, tannin-derived compounds (van Bergen *et al*. 2004). Suggested models of molecular structures for lignins and tannins (*e.g.*, Hernes *et al.* 2001, Heitner *et al.* 2010) could be indicative of higher aromaticity (CH_{ar}/CH_{al}) in lignin-like compounds, whereas the condensation degree of aromatic nuclei ($CH_{ar}/C = C$) is higher in tannin-like molecules (however see D'Angelo & Zodrow 2016).

Results indicate the highest contents of likely lignin-derived compounds occurred in the 48–51Pt and 52Ad samples, where values of the CH_{ar}/CH_{al} ratio are the highest of the entire data set (Table S1, Supplementary materials). Biomechanical studies on living plants demonstrated that

lignin content in stem tissues is related to the stiffness (*i.e.*, the Young's modulus of elasticity; *e.g.*, Niklas 1992, Alvarez-Clare 2005) rather than toughness (Lucas *at al.* 2000). This implies that in the *simonii* plant the petiole and the main bifurcation were more rigid than the rest of the frond as expected. In fact, mechanical support was the main physical function of the petiole, *e.g.*, reduction of the risk of breakage under self-weight or external loads.

Higher degrees of condensation of aromatic structures (CH_{ar}/C=C ratios) point to higher contents of tannin-derived or similar polymeric, phenolic structures. Bark and leaf tissues of many extant gymnosperms may have as much as 20% of tannins (*e.g.*, Hernes *et al.* 2001). IR-derived ratios from samples of Tk (cortex?), Pi's (from both the *simonii* frond and *simonii* specimens), Co, and Cf could be related to naphthalene-like compounds which probably were derived from diagenetically altered condensed tannins (proanthocyanidins) (*e.g.*, van Bergen *et al.* 1995, Boyce *et al.* 2003, de Leeuw *et al*. 2006). Plant synthesis of tannins and other phenols is linked to different functions, including nitrogen supply, when plants grow in nitrogen-poor soils, protection against herbivores and pathogens, and light screen against solar ultraviolet-B radiation (*e.g.*, Dustin & Cooper-Driver 1993, Berli *et al.* 2008, Seigler 2012).

Despite the likely presence of tannin-derived compounds in samples of Tk, Pi's (from all *simonii* specimens), Co and Cf, their relatively higher values of C=C cont, CH_{ar}/CH_{al}, and CH_{ar}/C=C ratios, are very likely related to polycyclic-aromatic hydrocarbons derived from terpenoid resins (*e.g.*, D'Angelo & Zodrow 2016). Similarly, oxygen- and aliphatic-rich structures including the relatively higher values of CH_2/CH_3, C=O cont, "A" factor, and "C" factor ratios could be in agreement with the probable presence of compounds derived from phenolic resins. Internally-produced resins (terpenoid-like compounds) play important roles for sequestering toxic chemicals that could then be released on attack by pests (Fahn 1979, Adinew 2014).

The more robust construction of the basal frond parts (*i.e.*, petiole and the basic bifurcation) is possibly linked to relatively higher contents of tannin- and lignin-derived compounds. Slender and less rigid morphologies characterizing the most distal parts of the frond are likely related to relatively higher contributions of aliphatics (*e.g.*, resin-like structures). Finally, polymeric compounds as those mentioned above, and some others, are mixed in unknown proportions, and were widely distributed throughout the frond of the once-living plant.

Architecturally emended *N. ovata* frond

The impetus for it stems from the long linear, unipinnate specimen 92-243 (Fig. 12) that does not fit the morphological characteristics of the intercalary form "*N. triangularis*". Moreover, we have no evidence from the *simonii* frond of the homology depicted by Laveine (1997, Fig. 12) of pinnae located directly below and above the main bifurcation, though the reconstructed frond (Zodrow & Cleal 1988, text-fig. 10) shows such without scale. Also, the specimen 92-243 exceeds by at least 6 cm the longest 9 cm ultimate pinna in the *simonii* frond, which suggests, as one alternative, that the PUr's would have to be much more widely spaced to accommodate such larger ultimate pinna. Additional impetus is specifically based on the micromorphological results regarding APUr and its size-invariant epidermis over a distance of 65 cm. This assumes that hypodermal structures vary in size with length. We therefore propose a not unreasonable 4-m frond with cyclopteroid leaflets situated above and below the main bifurcation, and also complex pinnate structures below the main bifurcation that conjecturally are homologous with intercalary pinnate structures in the main rachides (APUr's). Our biomechanical arguments based on the likely presence of tannin-, and lignin-derived compounds, indicating a relatively higher degree of rigidity for the bifurcation supports the hypothesis for a relatively large frond structure.

We were not successful in extracting informative cuticles from associated aphlebian fossils, and await confirmation from future experiments that would confirm sinusoidal patterns (equally for integumentary tissue from attached *N. ovata* ovules).

Fractal-taxonomic parameter

It includes the proposition that adaxial [pinnule] laminae in this frond, above and below the main bifurcation, are characterized by a certain sinusoidal cell-wall pattern, as indeed they are. But these patterns are present in many other Carboniferous species as well which begs the question of how to objectively species-differentiate these patterns? The quantitative approach suggested by fractal geometry is suggestive, which in this study has shown a narrow range of fractal dimensions (1.2 to 1.4), including in cyclopteroids. We caution that the converse is not necessarily true (Preen *et al.*, unpublished data), *i.e.*, a fractal dimension of 1.2 to 1.4 does not mean it is *N. ovata*.

Conclusions

The medullosalean species *N. ovata* is probably the most comprehensively studied Carboniferous plant fossil from the point-of-view of Pangaean distribution, vertical distribution in the Carboniferous, compression/epidermal morphology, frond architecture, relationship between morphology and chemistry, and autecology. Contributory insights

from the present study include a first comprehensive frond and cyclopteroid micromorphology co-ordinated with chemistry, cyclopteroid forms, distribution of appendages, stomata and secretory organs, vitrain rodlets in the medullosalean trunk, and new insights into the potential of fractal taxonomy. Most important, a tripartite epidermal Aufbau is recognized for the *simonii* frond, and proposed for medullosaleans. This all is realized through large and well-preserved (lower Ro%) study specimens of *N. ovata* var. *simonii*. Consequently, conclusions are reached highlighting/implying hypotheses of pinnate segmentation or polymorphism below and above the main bifurcation, based on defensible chemical affinity that is unorthodox according to current architectural thought. Implicit are questions pertaining to what is and how to define cyclopteroids, functionality? Are *N. ovata* varieties dependent on positions in one mother frond, originated from different stages over the lifetime of the plant, or something else? And can *N. ovata s.l.* be grouped as a natural species in the light of what is now known about it? Points of research interest are briefly summarized.

(1) Chemical investigation opened new frond-architectural theories which were not possible from morphological studies alone, particularly if based on fragmentary material. Foliar segmentation on petioles and the main rachis is indubitably more complex than previously hypothesized, and likely the case for medullosalean seed ferns generally?

(2) Florin's arguments for cyclopteroid-pinnule homology [neuropteroids] are not contradicted by our specimens.

(3) Single, entire-margined cyclopteroid leaflets probably grew on the proximal frond position. Not ruled out can be pinnate, fimbriate-cyclopteroid structures with a rather short petiole.

(4) But fortuitous finds are necessary to clarify the frond positions of the fimbriate and entire-margined cyclopteroid leaflets.

(5) Cyclopteroid-leaflet cuticles, relative to those of pinnules, are difficult to obtain because of coalification differences that are known to occur over a frond.

(6) The previously postulated 2-meter long frond, is "resized" to probably double that size, considering that common, ultimate pinnae of unknown frond location could exceed 20 cm, and that the sizes of the epidermal morphology remained virtually unchanged over the 65-cm antepenultimate rachis.

(7) Idioblastic features are currently undervalued in a number of questions, including taxonomy and autecology.

(8) Autecologically, the chemical data probably signal that the *N. ovata* plant may have been adapted to open, wet habitats with likely nitrogen-poor soil and considerable light availability. Secretory organs probably provided defensive chemicals against herbivory, and cutinization, lignifications, or tannin and resin concentrations reduced palatability or nutritional value.

(9) For an unbiased autecological evaluation, availability of larger structures is one prerequisite, another is knowledge of palaeosol conditions.

(10) A complete cuticular analysis, it is suggested, should include studies not only of the freed compression, but also of the sludge from the rock-matrix in which it was entombed.

(11) In effect, our experimental approach implies a paradigmatic shift in the study and taxonomy of medullosalean fronds, where chemistry is related to architecture.

Acknowledgement

We are indebted and thank colleagues for the use of equipment and other research material including data and literature: Dale Keefe, Molecular Spectroscopy Laboratory (FTIR spectrometer and consumables), Martha Jones, Biology Department (Nomarski phase-contrast microscope), and James Preen, Department of Mathematics (fractal analysis and interpretation), Cape Breton University; Maria Mastalerz, Indiana Geological Survey, Indiana University (vitrinite reflectance data); Gordon Brown, Earth Sciences, Dalhousie University, Earth Sciences (thin section preparation); and Christian Pott, Naturhistoriska Riksmuseet, Palaeobotany, Stockholm (Florin's papers and loan of his original slide of *Cyclopteris* sp., pl. 10, figs 3–12). We acknowledge the two journal reviewers (one anonymous) for their efforts and appreciate the time they spent on this MS, particularly Robert H. Wagner (Córdoba) for his detailed suggestions to improve style and presentation. Our cordial thanks to the Editor-in-Chief of the Bulletin of Geosciences for agreeing to cover the cost of color printing.

References

Adinew, B. 2014. GC-MS and FT-IR analysis of constituents of essential oil from *Cinnamon* bark growing in south-west Ethiopia. *International Journal of Herbal Medicine 1(6)*, 22–31.

Alvarez-Clare, S. 2005. *Biomechanical properties of tropical tree seedlings as a functional correlate of shade tolerance*. xii + 83 pp. MSc. thesis, University of Florida, Florida.

Barthel, M. 1962. Epidermisuntersuchungen an einigen inkohlten Pteridospermenblättern des Oberkarbons und Perms. *Geologie 11, Beiheft 33*, 1–140.

Barthel, M. 1966. Johann Georg Bornemann – Begründer der Kutikularanalyse. *Hallesches Jahrbuch Mitteldeutschlands Erdgeschichte 7*, 7–10.

Beeler, H.E. 1983. Anatomy and frond architecture of *Neuropteris ovata* and *N. scheuchzeri* from the Upper Pennsylvanian of the Appalachian Basin. *Canadian Journal of Botany 61(9)*, 2352–2368. DOI 10.1139/b83-259

Bell, W.A. 1938. Fossil Flora of Sydney Coalfield, Nova Scotia. *Geological Survey of Canada Memoir 215*, 1–334. DOI 10.4095/101646

Benítez, J., Matas, A.J. & Heredia, A. 2004. Molecular characterization of the plant biopolymer cutin by AFM and spectroscopic techniques. *Journal of Structural Biology 147*, 179–184. DOI 10.1016/j.jsb.2004.03.006

Van Bergen, P.F., Blokker, P., Collinson, M.E., Sinninghe Damsté, J.S. & De Leeuw, J.W. 2004. Structural biomacromolecules in plants: what can be learnt from the fossil record?, 133–154. *In* Hemsley, A.R. & Poole, A.I. (eds) *The evolution of plant physiology*. Elsevier Academy Press, Oxford.

Van Bergen, P.F., Collinson, M.E., Scott, A.C. & De Leeuw, J.W. 1995. Unusual resin chemistry from Upper Carboniferous pteridosperm resin rodlets, 149–169. *In* Anderson, K.B. & Crelling, J.C. (eds) *Amber, resinite and fossil resins. Symposium Series 617*. American Chemical Society, Washington D.C.

Berli, F., D'Angelo, J.A., Cavagnaro, B., Bottini, R., Wuilloud, R. & Silva, M. 2008. Phenolic composition in grape (*Vitis vinifera* L. Cv. Malbec) ripened with different solar UV-B radiation levels by capillary zone electrophoresis. *Journal of Agricultural Food Chemistry 56*, 2892–2898. DOI 10.1021/jf073421+

Bertrand, P. 1930. *Études des gîtes minéraux de la France. Bassin houiller de la Sarre et de la Lorraine. I. Flore fossile. 1er fascicule: Neuroptéridées.* 58 pp. Imprimerie L. Danel, Lille.

Bode, H. 1958. Die floristische Gliederung des Oberkarbons der Vereinigten Staaten von Nordamerica. *Zeitschrift der Deutscher Geologischen Gesellschaft 110*, 217–259.

Boyce, C.K., Cody, G.D., Fogel, M.L., Hazen, R.M., Alexander, C.M. O'D. & Knoll, A.H. 2003. Chemical evidence for cell wall lignification and the evolution of tracheids in early Devonian plants. *International Journal of Plant Science 164*, 691–702. DOI 10.1086/377113

Braune, W., Leman, A. & Taubert, H. 1999. *Pflanzenanatomisches Praktikum I. 8th edition*. 368 pp. Spektrum Akademischer Verlag, Heidelberg.

Brown, C.A. 1960. *Palynological techniques*. 188 pp. C.A. Brown, publisher, Baton Rouge, Louisiana.

De Candolle, A.P. 1816. *Essai sur les propriétés médicales des plantes, comparées avec leurs forms extérieures et leur classification, 2nd edition, revue et augmentée*. Crochard, Paris. DOI 10.5962/bhl.title.112422

Chen, Y., Zou, C., Mastalerz, M., Hu, S., Gasaway, C. & Tao, X. 2015. Applications of micro-Fourier Transform Infrared spectroscopy (FTIR) in the geological sciences - A review. *International Journal of Molecular Sciences 15*, 30223–302550. DOI 10.3390/ijms161226227

Cleal, C.J. & Shute, C.H. 1995. A synopsis of neuropteroid foliage from the Carboniferous and Lower Permian of Europe. *Bulletin of the British Museum (Natural History), Geology Series 51*, 1–52.

Cleal, C.J. & Shute, C.H. 2012. The systematic and palaeoecological value of foliage anatomy in Late Palaeozoic medullosalean seed-plants. *Journal of Systematic Palaeontology 10*, 765–800. DOI 10.1080/14772019.2011.634442

Cleal, C.J. & Thomas, B.A. 1994. *Plant fossils of the British Coal Measures*. 222 pp. Palaeontological Association, London.

Cleal, C.J. & Zodrow, E.L. 1989. Epidermal structure of some medullosalean *Neuropteris* foliage from the Middle and Upper Carboniferous of Canada and Germany. *Palaeontology 32*, 837–882.

Cleal, C.J., Zodrow, E.L. & Mastalerz, M. 2010. An association of *Alethopteris* foliage, *Trigonocarpus* ovules and *Bernaultia*-like pollen organs from the Middle Pennsylvanian of Nova Scotia, Canada. *Palaeontographica, Abteilung B 283*, 73–97.

Colthup, N.B., Daly, L.H. & Wiberley, S.E. 1990. *Introduction to infrared and Raman spectroscopy*. 547 pp. Academic Press, New York.

D'Angelo, J.A. 2006. Analysis by Fourier transform infrared spectroscopy of *Johnstonia* (Corystospermales, Corystospermaceae) cuticles and compressions from the Triassic of Cacheuta, Mendoza, Argentina. *Ameghiniana 43*, 669–685.

D'Angelo, J.A., Escudero, L., Volkheimer, W. & Zodrow, E.L. 2011. Chemometric analysis of functional groups in fossil remains of the *Dicroidium* flora (Cacheuta, Mendoza, Argentina): Implications for kerogen formation. *International Journal of Coal Geology 87*, 97–111. DOI 10.1016/j.coal.2011.05.005

D'Angelo, J.A. & Zodrow, E.L. 2011. Chemometric study of functional groups in different layers of *Trigonocarpus grandis* ovules (Pennsylvanian seed fern, Canada). *Organic Geochemistry 42*, 1039–1054. DOI 10.1016/j.orggeochem.2011.06.022

D'Angelo, J.A. & Zodrow, E.L. 2015. Chemometric study of structural groups in medullosalean foliage (Carboniferous, fossil Lagerstätte, Canada): Chemotaxonomic implications. *International Journal of Coal Geology 138*, 42–54. DOI 10.1016/j.coal.2014.12.003

D'Angelo, J.A. & Zodrow, E.L. 2016. 3-D chemical map and a theoretical life model for *Neuropteris ovata* var. *simonii* index fossil Asturian, Late Pennsylvanian, Canada). *International Journal of Coal Geology 153*, 12–27. DOI 10.1016/j.coal.2015.11.007

D'Angelo, J.A., Zodrow, E.L. & Mastalerz, M. 2012. Compression map, functional groups and fossilization: A chemometric approach (Pennsylvanian neuropteroid foliage, Canada). *International Journal of Coal Geology 90–91*, 149–155. DOI 10.1016/j.coal.2011.11.009

Darrah, W.C. 1969. *A critical review of the Upper Pennsylvanian floras of Eastern United States with notes on the Mazon*

Creek flora of Illinois. Privately printed. Library of Congress Catalog Card Number 74-113602. USA.

Dustin, C. & Cooper-Driver, G. 1993. Changes in phenolic production in the hay-scented fern (*Dennstaedtia punctilobula*) in relation to resource availability. *Biochemical Systematics and Ecology 20*, 99–106. DOI 10.1016/0305-1978(92)90096-V

Fahn, A. 1979. *Secretory tissues in plants*. 302 pp. Academic Press, New York.

Florin, R. 1925. Zur Kenntnis einiger Cyclopteriden des Oberkarbons. *Geologiska Föreningens i Stockholm Förhandlingar 47*, 223–244. DOI 10.1080/11035892509454044

Forgeron, S., Mackenzie, B. & Macpherson, K. 1986. The effects of geological features on coal mining, Sydney coalfield, Nova Scotia. *CIM Bulletin 79(891)*, 79–87.

Ganz, H. & Kalkreuth, W. 1987. Application of infrared spectroscopy to the classification of kerogen types and the evolution of source rock and oil shale potentials. *Fuel 66*, 708–711. DOI 10.1016/0016-2361(87)90285-7

Gibling, M.R., Langenberg, W., Kalkreuth, W.D., Waldron, J.W.F., Courtney, R., Paul, J. & Grist, A.M. 2002. Deformation of Upper Carboniferous coal measures in the Sydney Basin: evidence for late Alleghanian tectonism in Atlantic Canada. *Canadian Journal of Earth Sciences 39*, 79–93. DOI 10.1139/e01-062

Gothan, W. 1913. Die Oberschlesische Steinkohlenflora. 1. Teil. Farne und farnähnliche Gewächse. *Abhandlungen der Königlich Preussischen Geologischen Landesanstalt, Neue Folge 75*.

Gothan, W. 1916. Über die Epidermen einiger Neuropteriden des Carbons. *Jahrbuch der Königlich Preussischen Geologischen Landesanstalt 35*, *Teil II*, 373–381.

Greshoff-Haag, M. 1893. Gedanken über Pflanzenkräfte und phytochemische Verwandtschaft, *Berichte der Pharmaceutischen Gesellschaft 3,* 191–204.

Guo, Y. & Bustin, R.M. 1998. Micro-FTIR spectroscopy of liptinite macerals in coal. *International Journal of Coal Geology 36*, 259–275. DOI 10.1016/S0166-5162(97)00044-X

Hacquebard, P.A. 1984. Coal rank changes in the Sydney and Pictou coalfields of Nova Scotia; cause and economic significance. *CIM Bulletin 77*, 33–40.

Heggie, M. & Zodrow, E.L. 1994. Fractal lobatopterid frond (Upper Carboniferous marattialean tree fern). *Palaeontographica, Abteilung B 232*, 35–57.

Hegnauer, R. 1986. Phytochemistry and plant-taxonomy – An essay on the chemotaxonomy of higher plants. *Phytochemistry 25*, 1519–1535. DOI 10.1016/S0031-9422(00)81204-2

Heitner, C., Dimmel, D. & Schmidt, J.A. 2010. *Lignin and Lignans: Advances in chemistry*. 683 pp. CRC Press, Taylor & Francis Group. Florida.

Heredia-Guerrero, J.A., Benetíz, J.J., Domínguez, E., Bayer, I.S., Cingolani, R., Athanassiou, A. & Heredia, A. 2014. Infrared and Raman spectroscopic features of plant cuticles: a review. *Frontiers in Plant Science 5(305)*, 1–14. DOI 10.3389/fpls.2014.00305

Hernes, P.J., Benner, R., Cowie, G., Goñi, M.A., Bergamaschi, B.A. & Hedges, J.I. 2001. Tannin diagenesis in mangrove leaves from a tropical estuary: A novel molecular approach. *Geochimica et Cosmochimica Acta 65*, 3109–3122. DOI 10.1016/S0016-7037(01)00641-X

Hoffmann, F. 1826. Über die Pflanzenreste des Kohlengebirges von Ibbenbühren und vom Piesberge bei Osnabrück, 150–160. *In* Keferstein, C. (ed.) *Teutschland geognostisch-geologisch dargestellt und mit Charten und Zeichnungen erläutert 4(2)*.

Jongmans, W.J. 1952. Some problems on Carboniferous stratigraphy, 295–306. *In 3e Congrès pour l'Avancement des Études de Stratigraphie et de Géologie du Carbonifère, Heerlen 25–30 Juin, 1951*. *Compte Rendu 1*. Ernest van Aelst, Maestricht.

Khan, A.M., Bera, S., Ghosh, R., Spicer, R.A. & Spicer, T.E.V. 2015. Leaf cuticular morphology of some angiosperm taxa from the Siwalik sediments (middle Miocene to lower Pleistocene) of Arunachal Pradesh, eastern Himalaya: Systematic and palaeoclimatic implications. *Review of Palaeobotany and Palynology 214*, 9–26. DOI 10.1016/j.revpalbo.2014.10.008

Klassen, H. (ed.) 1984. *Geologie des Osnabrücker Berglandes*. 672 pp. Naturwissenschaftliches Museum, Osnabrück.

Krumbein, W.C. & Garrels, R.M. 1952. Origin and classification of chemical sediments in terms of pH and oxidation-reduction potentials. *Journal of Geology 52*, 1–33. DOI 10.1086/625929

Laveine, J.P. 1967. Contribution à l'étude de la flore du terrain houiller. Les Neuroptéridées du Nord de la France: 1. Flore fossiles, 5e fascicule. *Études Géologiques pour l'Atlas de Topographie Souterraine, Houillères du bassin du Nord et du Pas-de-Calais. Service géologique 1(5)*, 1–344.

Laveine, J.P. 1977. Report on the Westphalian D, 71–81. *In* Holub, V.M. & Wagner, R.H. (eds) *Symposium on Carboniferous stratigraphy*. Czech Geological Survey, Prague.

Laveine, J.P. 1997. Synthetic analysis of the Neuropterids. Their interest for the decipherment of Carboniferous palaeogeography. *Review of Palaeobotany and Palynology 95*, 155–189. DOI 10.1016/S0034-6667(96)00033-4

Laveine, J.P., Kahlert, E. & Schultka, S. 2005. Frond architecture of two specimens of the pteridosperm *Laveineopteris rarinervis* from the Late Carboniferous (early Westphalian D) of Piesberg near Osnabrück (Germany): morphological implications. *Revue de Paléobiologie 24*, 489–504.

De Leeuw, J.W., Versteegh, G.J.M. & Van Bergen, P.F. 2006. Biomacromolecules of algae and plants and their fossil analogs. *Plant Ecology 182*, 209–233. DOI 10.1007/s11258-005-9027-x

Lin, R. & RITZ, G.P. 1993a. Reflectance FT-IR microspectroscopy of fossil algae contained in organic-rich shale. *Applied Spectroscopy 47*, 265–271. DOI 10.1366/0003702934066794

Lin, R. & Ritz, G.P. 1993b. Studying individual macerals using i.r. microspectroscopy, and implications on oil versus gas/condensate proneness and "low-rank" generation. *Or-*

ganic Geochemistry 20, 695–706.
DOI 10.1016/0146-6380(93)90055-G

Lucas, P.W., Turner, I.M., Dominy, N.J. & Yamashita, N. 2000. Mechanical defenses to herbivory. *Annals of Botany 86*, 913–920. DOI 10.1006/anbo.2000.1261

Lyons, P.C., Finkelman, R.B., Thompson, C.L., Brown, F.W. & Hatcher, P.G. 1982. Properties, origin and nomenclature of rodlets of the inertinite maceral group in coals of the Central Appalachian Basin, U.S.A. *International Journal of Coal Geology 1*, 313–346.
DOI 10.1016/0166-5162(82)90019-2

Lyons, P.C. & Laveine, J.P. 2005. Association of entire orbicular cyclopterids with *Neuropteris ovata* pinnate foliage from the Late Pennsylvanian (Stephanian) of West Virginia, USA: taxonomical implications. *Revue de Paléobiologie 24*, 505–514.

Lyons, P.C., Orem, W.H., Mastalerz, M., Zodrow, E.L., Vieth-Redemann, A. & Bustin, R.M. 1995. ^{13}CMR, micro-FTIR and fluorescence spectra, and pyrolysis-gas chromatograms of coalified foliage of late Carboniferous medullosan seed ferns, Nova Scotia, Canada: Implications for coalification and chemotaxonomy. *International Journal of Coal Geology 27*, 227–248.
DOI 10.1016/0166-5162(94)00024-T

Mandelbrot, B.B. 1983. *The fractal geometry of nature*. 498 pp. W.H. Freeman & Co., New York.

Miranda, V., Baker, N.R. & Long, S.P. 1981. Anatomical variation along the length of the *Zea mays* leaf in relation to photosynthesis. *New Phytologist 88*, 595–605.
DOI 10.1111/j.1469-8137.1981.tb01735.x

Niklas, K.J. 1992. *Plant Biomechanics: An engineering approach to plant form and function*. 622 pp. University of Chicago Press, Chicago.

De Oliveira Plotze, R., Falvo, M., Pádua, J.G., Bernacci, L.C., Vieira, M.L.C., Oliveira, G.C.X. & Bruno, O.M. 2005. Leaf shape analysis using multiscale Minkowski fractal dimension, a new morphometric methods: a study with *Passiflora* (Passifloraceae). *Canadian Journal of Botany 83*, 287–301. DOI 10.1139/b05-002

Petersen, H.I. & Nytoft, H.P. 2006. Oil generation capacity of coals as a function of coal age and aliphatic structure. *Organic Geochemistry 37*, 558–583.
DOI 10.1016/j.orggeochem.2005.12.012

Petersen, H.I., Rosenberg, P. & Nytoft, H.P. 2008. Oxygen groups in coals and alginite-rich kerogen revisited. *International Journal of Coal Geology 74*, 93–113.
DOI 10.1016/j.coal.2007.11.007

Rochleder, F. 1854. Phytochemie, 257–308. *Über den Zusammenhang zwischen der Form and Zusammensetzung der Gewächse, 3. Abschnitt*. Wilhelm Engelmann, Leipzig.

Rothwell, G.W. 1985. The role of comparative morphology and anatomy in interpreting the systematics of fossil gymnosperms. *The Botanical Review 51*, 319–327.
DOI 10.1007/BF02861078

Saltzwedel, K. 1968. *Revision der Imparipteris ovata (Hoffmann) Gothan, ihre Lebensdauer und stratigraphische Bedeutung in den westeuropäischen Varisziden*. 169 pp. Inaugural Dissertation, Universität von Münster, Münster.

Saltzwedel, K. 1969. Revision der *Imparipteris ovata* (Hoffmann) Gothan. 1. Teil: Typus- und Typoid-Material vom *locus typicus*. *Argumenta Palaeobotanica 3*, 131–162.

Seigler, D.S. 2012. *Plant secondary metabolism*. 759 pp. Springer Science & Business Media, New York.
DOI 10.1007/978-1-4615-4913-0

Shute, C.H. & Cleal, C.J. 2002. Ecology and growth habit of *Laveineopteris*: a gymnosperm from the Late Carboniferous tropical rain forests. *Palaeontology 45*, 943–972.
DOI 10.1111/1475-4983.00270

Šimůnek, Z & Cleal, C.J. 2016. The systematic and palaeoecological significance of *Neuropteris ovata* (Medullosales) cuticles from the Stephanian Stage of the Puertollano Basin, Spain. *Spanish Journal of Palaeontology 31*, 231–244.

Smith, B.C. 1996. *Fundamentals of Fourier transform infrared spectroscopy*. 202 pp. CRC Press, New York.

Smith, T.G., Lange, G.D. & Marks, W.B. 1996. Fractal methods and results in cellular morphology – dimensions, lacunarity and multifractals. *Journal of Neuroscience Methods 69*, 123–136. DOI 10.1016/S0165-0270(96)00080-5

Stace, C.A. 1984. The taxonomic importance of the leaf surface, 67–94. *In* Heywood, H. & Moore, D.M. (eds) *Current concepts in plant taxonomy. Systematics Association, London (Special Volume 25)*. Clarendon Press, Oxford.

Stafleu, F.A. 1966. *Brongniart's Histoire des Végétaux fossiles*. 2 vols 1828–1837. Reimpression A. Asher & Co., Amsterdam 1965.

Traverse, A. 2008. *Paleopalynology. Second edition*. 813 pp. Springer, Berlin. DOI 10.1007/978-1-4020-5610-9

Wagner, R.H. 1984. Megafloral zones of the Carboniferous. *Compte Rendu 9e Congrès de stratigraphie et de géologie du Carbonifère (Washington-Urbana, 1979) 2*, 109–134.

Werner-Zwanziger, U., Banghao Chen, & Zodrow, E.L. 2009. ^{13}C NMR study of gymnospermous cuticles and associated coals from Late Pennsylvanian seed ferns and cordaites. *Poster 341, 50th Experimental Nuclear Magnetic Resonance Conference, Asilomar, CA, USA, March 29–April 3, 2009.*

Westad, F. 2002. Parsimonious models in chemometrics. *The North American Chapter of the International Chemometrics Society, Newsletter 22*, 10–13.

Wheeler, Q.D. 2008. *The new taxonomy*. 256 pp. CRC Press, New York. DOI 10.1201/9781420008562

Zodrow, E.L. & Cleal, C.J. 1985. Phyto- and chronostratigraphical correlations between the late Pennsylvanian Morien Group (Sydney, Nova Scotia) and the Silesian Pennant Measures (south Wales). *Canadian Journal of Earth Sciences 22*, 1465–1473. DOI 10.1139/e85-152

Zodrow, E.L. & Cleal, C.J. 1988. The structure of the Carboniferous pteridosperm frond *Neuropteris ovata* Hoffmann. *Palaeontographica B 208*, 105–124.

Zodrow, E.L. & D'Angelo, J.A. 2013. Digital compression maps: an improved method for studying Carboniferous foliage. *Atlantic Geology 49*, 126–130.
DOI 10.4138/atlgeol.2013.006

Zodrow, E.L., D'Angelo, J.A., Mastalerz, M. & Keefe, D. 2009. Compression-cuticle relationship of seed ferns: Insights from liquid-solid states FTIR (Late Palaeozoic-Early Mesozoic, Canada-Spain-Argentina). *International Journal of Coal Geology 79*, 61–73. DOI 10.1016/j.coal.2009.06.001

Zodrow, E.L., D'Angelo, J.A., Taylor, W.A., Catenali, T., Heredia-Guerrero, J.A. & Mastalerz, M. 2016. Secretory organs: Implications for lipoid taxonomy and kerogen formation (seed ferns, Pennsylvanian, Canada). *International Journal of Coal Geology 167*, 184–200. DOI 10.1016/j.coal.2016.10.004

Zodrow, E.L., D'Angelo, J.A., Werner-Zwanziger, U. & Banghao, C. 2014. Hair-trichomes-files, and spectrochemistry of *Macroneuropteris scheuchzeri* (Basal Cantabrian, Sydney Coalfield, Canada). *Palaeontographica B 290*, 141–153.

Zodrow, E.L., Helleur, R., Werner-Zwanziger, U., Banghao, C. & D'Angelo, J.A. 2013. Spectrochemical study of coalified *Trigonocarpus grandis* (Pennsylvanian tree-fern ovule, Canada): Implications for fossil-organ linkage. *International Journal of Coal Geology 109–110*, 24–35. DOI 10.1016/j.coal.2013.01.013

Zodrow, E.L. & Mastalerz, M. 2001. Chemotaxonomy for naturally macerated tree-fern cuticles (Medullosales and Marattiales), Carboniferous Sydney and Mabou Sub-Basins, Nova Scotia, Canada. *International Journal of Coal Geology 47*, 255–275. DOI 10.1016/S0166-5162(01)00045-3

Zodrow, E.L. & Mastalerz, M. 2009. A proposed origin for fossilized Pennsylvanian plant cuticles by pyrite oxidation (Sydney Coalfield, Nova Scotia, Canada). *Bulletin of Geosciences 84(2)*, 227–240. DOI 10.3140/bull.geosci.1094

Zodrow, E.L., Mastalerz, M., Werner-Zwanziger, U. & D'Angelo, J.A. 2010. Medullosalean fusain trunk from the roof rocks of a coal seam: Insight from FTIR and NMR (Pennsylvanian Sydney Coalfield, Canada. *International Journal of Coal Geology 82*, 116–124. DOI 10.1016/j.coal.2010.02.006

Zodrow, E.L., Šimůnek, Z. & Bashforth, A.R. 2000. New cuticular morphotypes of *Cordaites principalis* from the Canadian Carboniferous Maritimes Basin. *Canadian Journal of Botany 78(2)*, 135–148. DOI 10.1139/b00-010

Supplementary materials

S1 Studies on *Neuropteris ovata* (Hoffmann) from the Sydney Coalfield, Canada

These include the biostratigraphical correlation of Sydney Coalfield (Sub-Basin of Maritimes Carboniferous Basin; Roliff 1962, Calder 1998, Gibling *et al*. 2008) with the Pennant Measures of South Wales (Zodrow & Cleal 1985); reconstruction of the *N. ovata* frond based on the 65-cm frond section (Zodrow & Cleal 1988, text-fig. 10); medullosalean cuticular analysis Canada-Saarland (Cleal & Zodrow 1989) and proposal for a new neuropterid taxonomy (Cleal *et al*. 1990); and the relationship of stomatal-density distribution and Late Carboniferous climate change (Cleal *et al*. 1999). These were followed by first-time applications of advanced spectrochemical methods to the study of *N. ovata* in an effort to elucidate biomolecular (cutin structure), and information and coalification pattern. Involved were Fourier transform infrared spectrometry (FTIR), carbon 13 nuclear magnetic resonance (^{13}C NMR), pyrolysis-gas chromatography/mass spectrometry (py-GC/MS), and fluorescence-spectral studies) (Lyons *et al*. 1995); investigating the relationship between chemistry (*i.e*., chemical structural groups) and the taxonomy of medullosalean Families (D'Angelo & Zodrow 2015); presenting a 3D chemical map and a theoretical life model for Zodrow & Cleal's (1988) reconstructed *N. ovata* frond (D'Angelo & Zodrow 2016); and by the present study.

S2 Maceration time, and information from liberated compression and its matrix

Maceration time for cuticles depends on the degree of coalification and thickness of compressions, which in turn is influenced by the degree of natural maceration. These have been demonstrated to be variable even in smaller 22-cm specimens (Zodrow & D'Angelo 2013). Important for assessing the influence of facies on the preservation of *N. ovata* were records of maceration time for compressed pinnules, and information from compression surfaces and epicuticular features left in the rock matrix after maceration.

Maceration procedure

Schulze's (1855) oxidative procedure (maceration or softening of coal) has been successfully, and continuous to be used by us to extract plant-fossil cuticles from compressions of the Sydney Coalfield for the past 26 years (Cleal & Zodrow 1989). Macerating pinnules from the *simonii* frond for 2 h 40 min, reduced to 1 h 5 min, 35 min, 25 min, 20 min, and to 10–15 min made little difference for separating ad- from abaxial surfaces, nor in the study quality of the cuticle, as at each time stage separation proved equally difficult to accomplish. At 5 min, a pinnule was clearly under-macerated for its preservation state, as insoluble

Table S1. Complete data set of semi-quantitative FTIR data from compressions as input matrix for the principal component (PCA) solutions, and ID for scores.

ID	CH_2/CH_3	CH_{al}/Ox	C=O/ C=C	C=O cont	C=C cont	CH_{al}/ C=C	"A"factor	"C" factor	CH_{al}/ C=O	CH_{ar}/ CH_{al}	CH_{ar}/ C=C
1Pi	2.5	0.78	0.03	0.01	0.45	1.73	0.63	0.026	64.9	0.27	0.46
2Pi	2.0	0.50	0.03	0.02	0.59	0.84	0.46	0.027	30.1	0.57	0.48
3Pi	2.5	0.54	0.02	0.01	0.56	0.96	0.49	0.021	45.5	0.49	0.47
4Pi	2.0	0.50	0.02	0.01	0.50	1.01	0.50	0.020	50.0	0.47	0.47
5Pi	1.9	0.50	0.02	0.01	0.49	1.01	0.50	0.021	47.2	0.45	0.45
6Pi	1.9	0.46	0.02	0.01	0.49	0.94	0.48	0.021	44.5	0.48	0.45
7Pi[b]	2.3	0.61	0.01	0.006	0.45	1.36	0.58	0.014	97.6	0.30	0.40
8Pi	2.2	0.58	0.01	0.006	0.43	1.34	0.57	0.013	99.9	0.32	0.42
9Pi	2.3	0.57	0.03	0.01	0.45	1.28	0.56	0.028	44.1	0.34	0.44
10Pi	1.9	0.52	0.02	0.01	0.48	1.07	0.52	0.021	49.4	0.38	0.40
11Pi	2.2	0.47	0.03	0.01	0.45	1.03	0.51	0.031	32.6	0.37	0.38
12Pin	2.1	0.56	0.02	0.009	0.48	1.17	0.54	0.018	64.2	0.36	0.42
29Tk	1.5	0.32	0.03	0.01	0.46	0.68	0.41	0.026	25.4	0.54	0.37
30Tk	1.6	0.32	0.03	0.01	0.44	0.72	0.42	0.031	22.2	0.60	0.43
31Tk	1.9	0.30	0.05	0.02	0.47	0.64	0.39	0.046	13.3	0.51	0.33
32Pi	1.9	0.44	0.01	0.006	0.56	0.79	0.44	0.010	75.9	0.50	0.40
33Pi	1.9	0.44	0.03	0.02	0.53	0.83	0.45	0.032	25.4	0.45	0.38
34Pi	1.9	0.47	0.04	0.02	0.49	0.97	0.49	0.035	26.8	0.41	0.40
35Pi	1.6	0.46	0.04	0.02	0.48	0.97	0.49	0.037	24.9	0.40	0.39
36Pi	2.1	0.41	0.02	0.01	0.51	0.81	0.45	0.022	36.9	0.49	0.39
37Pi	2.0	0.42	0.02	0.01	0.51	0.81	0.45	0.024	32.6	0.49	0.39
38Pi	2.0	0.42	0.02	0.01	0.52	0.80	0.44	0.024	32.9	0.51	0.41
39Pi	1.3	0.65	0.03	0.01	0.57	1.14	0.53	0.025	44.9	0.38	0.43
40Pi	1.4	0.53	0.02	0.01	0.59	0.90	0.47	0.019	46.9	0.42	0.38
41Pi	1.7	0.62	0.02	0.01	0.58	1.07	0.52	0.023	45.6	0.37	0.39
42Co	2.2	0.44	0.02	0.01	0.55	0.79	0.44	0.023	33.9	0.50	0.40
43Co	2.1	0.44	0.02	0.01	0.56	0.79	0.44	0.022	35.0	0.49	0.39
44Co	2.3	0.46	0.02	0.01	0.54	0.85	0.46	0.018	47.6	0.43	0.37
45Cf	3.6	0.67	0.10	0.07	0.48	1.39	0.58	0.12	10.2	0.09	0.12
46Cf	2.1	0.51	0.008	0.003	0.43	1.18	0.54	0.0075	155.9	0.24	0.28
47Cf	2.2	0.51	0.007	0.003	0.44	1.14	0.53	0.0071	160.8	0.29	0.33
48Pt	2.9	0.01	0.02	0.007	0.3	0.02	0.02	0.023	0.8	13.38	0.25
49Pt	2.6	0.01	0.04	0.01	0.27	0.02	0.02	0.042	0.5	18.47	0.37
50Pt	2.9	0.01	0.03	0.01	0.29	0.02	0.02	0.033	0.5	17.02	0.31
51Pt	2.7	0.01	0.04	0.01	0.35	0.02	0.02	0.037	0.5	18.72	0.33
52Ad	3.1	0.01	0.04	0.01	0.35	0.02	0.02	0.04	0.5	11.71	0.23

coaly matter was left (see D'Angelo *et al.* 2012, fig. 3C). In contrast, maceration time for the compressed pinnules from other *N. ovata* specimens was in the order of 5 h to 6 h, which produced cuticles with good separation quality, except for the specimen 07-6/15-5a. Increasing maceration from 3 h to 5 h, 8 h and 26 h did not improve separation capability as surfaces consistently remained "glued" together by intercostal mesophyll, which in effect is a coal precursor (Lyons *et al.* 1995). The lowest CH_2/CH_3 ratios recorded (1.3–1.7), and comparatively higher-than-usual levels of aromaticity C=C cont (0.57–0.59) for pinnules 39–41Pi underpin this observation (Table S1). When physically bared, these surfaces are seen to be well preserved, even if macerated for only 3h. Ultimate rachis (Ur) cuticles were generally mesophyll-free. Experimenting with cyclopteroid specimens (see also Florin 1925) showed that *Cycloptetris* sp. A,

Principal component solutions
PCA

Table S2. Input correlation matrix of eleven variables with unity in the principal diagonal.

	CH_2 / CH_3	CH_{al} / Ox	C=O / C=C	C=O cont	C=C cont	CH_{al} / C=C	"A" factor	C factor	CH_{al} / C=O	CH_{ar} / CH_{al}	CH_{ar} / C=C
CH_2 / CH_3	1	–0.354664	0.447546	0.391302	–0.578160	–0.279878	–0.449949	0.524591	–0.223275	0.546638	–0.632304
CH_{al} / Ox	–0.354664	1	–0.107635	0.179291	0.707633	0.972566	0.965913	–0.080283	0.540463	–0.862537	0.392132
C=O / C=C	0.447546	–0.107635	1	0.892480	–0.172540	–0.096810	–0.153855	0.976878	–0.580560	0.184620	–0.542563
C=O cont	0.391302	0.179291	0.892480	1	0.103270	0.163246	0.136544	0.930980	–0.359808	–0.107768	–0.498866
C=C cont	–0.578160	0.707633	–0.172540	0.103270	1	0.549976	0.707099	–0.169349	0.202645	–0.800313	0.458099
CH_{al} / C=C	–0.279878	0.972566	–0.096810	0.163246	0.549976	1	0.960856	–0.069218	0.605511	–0.829442	0.339126
"A" factor	–0.449949	0.965913	–0.153855	0.136544	0.707099	0.960856	1	–0.130150	0.572804	–0.940229	0.415883
C factor	0.524591	–0.080283	0.976878	0.930980	–0.169349	–0.069218	–0.130150	1	–0.534143	0.167391	–0.602787
CH_{al} / C=O	–0.223275	0.540463	–0.580560	–0.359808	0.202645	0.605511	0.572804	–0.534143	1	–0.470390	0.157338
CH_{ar} / CH_{al}	0.546638	–0.862537	0.184620	–0.107768	–0.800313	–0.829442	–0.940229	0.167391	–0.470390	1	–0.394449
CH_{ar} / C=C	–0.632304	0.392132	–0.542563	–0.498866	0.458099	0.339126	0.415883	–0.602787	0.157338	–0.394449	1

Table S2. Solution of PCA.

Variable	Component 1	Component 2	Component 3	Component 4	Component 5	Component 6	Component 7	Component 8	Component 9	Component 10	Component 11	
CH_2 / CH_3	–0.673903	0.267523	0.506177	–0.260666	–0.379292	–0.063121	–0.036775	–0.030024	–0.003468	0.002916	0.001652	1
CH_{al} / Ox	0.856333	0.457865	0.118642	–0.132283	–0.038955	0.058562	0.137210	0.019477	–0.001765	–0.030754	0.019407	1
C=O / C=C	–0.533402	0.800299	–0.161378	–0.058031	0.158307	0.054480	–0.002931	–0.124645	–0.044285	0.006062	0.004617	1
C=O cont	–0.270283	0.941500	–0.068234	0.046188	–0.022627	0.075571	–0.101779	0.126725	–0.033086	–0.000384	–0.000638	1
C=C cont	0.748765	0.273788	–0.407877	0.249001	–0.346668	0.115335	0.024835	–0.042000	0.005011	0.009384	–0.007140	1
CH_{al} / C=C	0.819623	0.449790	0.262983	–0.200868	0.082987	–0.025225	0.088841	0.006777	–0.014297	0.004479	–0.026720	1
"A" factor	0.896947	0.415698	0.092242	–0.051619	0.057098	–0.066197	–0.021753	0.008815	0.022242	0.051432	0.013234	1
C factor	–0.530888	0.835312	–0.073051	–0.034708	0.073332	0.027863	–0.019456	–0.015986	0.083003	–0.012960	–0.004993	1
CH_{al} / C=O	0.662124	–0.169764	0.677265	0.151166	0.077479	0.174470	–0.115295	–0.037759	0.005081	–0.006704	–0.000200	1
CH_{ar} / CH_{al}	–0.878729	–0.364233	0.068969	–0.155397	0.010835	0.227826	0.111228	0.032845	0.008106	0.026932	0.000017	1
CH_{ar} / C=C	0.655225	–0.368070	–0.434194	–0.475305	–0.009813	0.076249	–0.121336	–0.008826	0.003741	–0.006371	–0.000523	1
Eigenvalue	5.5037	3.25289	1.20233	0.47008	0.31287	0.12335	0.0803	0.0376	0.01079	0.00472	0.00137	11
Cumulative explained variance %	50.0337	79.6054	90.5357	94.8091	97.6534	98.7748	99.5047	99.8465	99.9446	99.9876	100	

even after 41 h 15 min maceration time, still had retained some mesophyll, but when it was cleared excellent topographical detail emerged for study. In contrast, *C. fimbriata*, 977-443 only yielded long-string-like costal-field cuticles. An important conclusion is the near-insolubility of mesophyllous remains by Schulze's procedure, implying a composition different from coal (vitrain).

Compressions and left-over rock matrices

Taxonomical observations if solely based on coalified compressions still attached to their rock matrices are likely morphologically biased, although cuticular work could assist in reducing that bias. We routinely study the liberated compressions floating in water to observe damage inflicted on them, if any (mechanical/plant-eating animals/mineral crystallization), framboidal-pyrite deposition, topographic appendages (trichomes/files), and the degree of coalification/natural maceration (the compression). Complementary to (two-dimensional) cuticular analysis are observations on the partially HF-digested rock matrices from which compressions were liberated. This may involve recovery of epicuticular features (trichomes, files) for example that were left in place in the rock sludge for correlation with structural holes found in the cuticle, provide material for spectrochemical analysis and scanning-electron microscopy that otherwise would not have been available (Zodrow *et al*. 2012, Zodrow 2014).

Table S4. Acceptable two-component solution of PCA. Abbreviation: * Variance explained by first 2 PC's (%).

Variable	Component 1	Component 2	Variance *
CH_2 / CH_3	–0.673903	0.267523	0.52571
CH_{al} / Ox	0.856333	0.457865	0.94295
C=O / C=C	–0.533402	0.800299	0.925
C=O cont	–0.270283	0.941500	0.95948
C=C cont	0.748765	0.273788	0.63561
CH_{al} / C=C	0.819623	0.449790	0.87409
"A" factor	0.896947	0.415698	0.97732
C factor	–0.530888	0.835312	0.97959
CH_{al} / C=O	0.662124	–0.169764	0.46723
CH_{ar} / CH_{al}	–0.878729	–0.364233	0.90483
CH_{ar} / C=C	0.655225	–0.368070	0.5648
Eigenvalue	5.5037	3.25289	8.75659
Cumulative explained variance %	50.0337	79.6054	

References

Calder, J.H. 1998. The Carboniferous of Nova Scotia, 261–302. *In* Blundel, D.J. & Scott, A.C. (eds) *Lyell: the Past is the Key to the Present. Geological Society of London, Special Publication 143*.

Cleal, J.C., James, R.M. & Zodrow, E.L. 1999. Variation in stomatal density in the Late Carboniferous gymnosperm frond *Neuropteris ovata*. *Palaios 14*, 180–185. DOI 10.2307/3515373

Cleal, C.J., Shute, C. & Zodrow, E.L. 1990. A revised taxonomy for Palaeozoic neuropterid foliage. *Taxon 39*, 486–492. DOI 10.2307/1223109

Cleal, C.J. & Zodrow, E.L. 1989. Epidermal structure of some medullosan *Neuropteris* foliage from the middle and upper Carboniferous of Canada and Germany. *Palaeontology 32*, 837–882.

D'Angelo, J.A. & Zodrow, E.L. 2015. Chemometric study of structural groups in medullosalean foliage (Carboniferous, fossil Lagerstätte, Canada). *International Journal of Coal Geology 138*, 42–54. DOI 10.1016/j.coal.2014.12.003

D'Angelo, J.A. & Zodrow, E.L. 2016. 3D chemical map and a theoretical life model for *Neuropteris ovata* var. *simonii* (index fossil, Asturian, Late Pennsylvanian, Canada). *International Journal of Coal Geology 153*, 12–27. DOI 10.1016/j.coal.2015.11.007

D'Angelo, J.A., Zodrow, E.L. & Mastalerz, M. 2012. Compression map, functional groups and fossilization: A chemometric approach (Pennsylvanian neuropteroid foliage, Canada). *International Journal of Coal Geology 90–91*, 149–155. DOI 10.1016/j.coal.2011.11.009

Florin, R. 1925. Zur Kenntnis einiger Cyclopteriden des Oberkarbons. *Geologiska Föreningens i Stockholm Förhandlingar 47*, 223–244. DOI 10.1080/11035892509454044

Gibling, M.R., Culshaw, N., Rygel, M.C. & Pascucci, V. 2008. The Maritimes Basin of Atlantic Canada: Basin creation and destruction in the collisional Zone of Pangea, 211–237. *In* Miall, A.D. (ed.) *Sedimentary Basins of the World. 5. The Sedimentary Basins of the United States and Canada*. Elsevier.

Lyons, P.C., Orem, W.H., Mastalerz, M., Zodrow, E.L., Vieth-Redemann, A. & Bustin, R.M. 1995. ^{13}CMR, micro-FTIR and fluorescence spectra, and pyrolysis-gas chromatograms of coalified foliage of late Carboniferous medullosan seed ferns, Nova Scotia, Canada: Implications for coalification and chemotaxonomy. *International Journal of Coal Geology 27*, 227–248. DOI 10.1016/0166-5162(94)00024-T

Roliff, W.A. 1962. The Maritimes Carboniferous Basin of eastern Canada. *Proceedings of the Geological Association of Canada 14*, 21–41.

Schulze, F. 1855. Bemerkungen über das Vorkommen wohlerhaltener Cellulose in Braunkohle and Steinkohle. *Verhandlungen der Königlich Preussischen Akademie der Wissenschaft zu Berlin*, 676–678.

Zodrow, E.L. 2014. Molecular self-assembly: Hypothesized for "hair" of *Macroneuropteris scheuchzeri* (Pennsylvanian-age seed fern). *International Journal of Coal Geology 121*, 14–18. DOI 10.1016/j.coal.2013.11.002

Zodrow, E.L. & Cleal, C.J. 1985. Phyto- and chronostratigraphical correlations between the late Pennsylvanian Morien Group (Sydney Nova Scotia) and the Silesian Pennant Measures (south Wales). *Canadian Journal of Earth Sciences 22*, 1465–1473. DOI 10.1139/e85-152

Zodrow, E.L. & Cleal, C.J. 1988. The structure of the Carboniferous pteridosperm frond *Neuropteris ovata* Hoffmann. *Palaeontographica, Abteilung B 208*, 105–124.

Zodrow, E.L. & D'Angelo, J.A. 2013. Digital compression maps: an improved method for studying Carboniferous foliage. *Atlantic Geology 49*, 126–130. DOI 10.4138/atlgeol.2013.006

Zodrow, E.L., D'Angelo, J.A., Helleur, R. & Šimůnek, Z. 2012. Functional groups and common pyrolysates products of *Odontopteris cantabrica* (index fossil for the Cantabrian Substage, Carboniferous). *International Journal of Coal Geology 100*, 40–50. DOI 10.1016/j.coal.2012.06.002